

Notable Events

# Notable events of Kamchatka in 2013

V. N. Chebrov *et. al.*

Kamchatka Branch of Geophysical Survey  
of Russian Academy of Sciences (RAS)

Petropavlovsk-Kamchatsky

Excerpt from the

Summary of the Bulletin of the International Seismological Centre

# 1

## Notable Events

### 1.1 Notable events of Kamchatka in 2013

V. N. Chebrov<sup>1</sup> (1949-2016), D. V. Chebrov<sup>1</sup>, I. R. Abubakirov<sup>1</sup>, A. Yu. Chebrova<sup>1</sup>, A. A. Gusev<sup>1&2</sup>, E. M. Guseva<sup>1</sup>, D. V. Droznin<sup>1</sup>, S. Ya. Droznina<sup>1</sup>, E. M. Ivanova<sup>1</sup>, N. M. Kravchenko<sup>1</sup>, Yu. A. Kugaenko<sup>1</sup>, A. V. Lander<sup>3</sup>, E. A. Matveenko<sup>1</sup>, S. V. Mitushkina<sup>1</sup>, D. A. Ototiuk<sup>1</sup>, V. M. Pavlov<sup>1</sup>, A. A. Raevskaya<sup>1</sup>, V. A. Saltykov<sup>1</sup>, A. A. Skorkina<sup>1</sup>, N. N. Titkov<sup>1</sup>



Viktor N. Chebrov (1949-2016)



Danila V. Chebrov

1. Kamchatka Branch of Geophysical Survey of Russian Academy of Sciences (RAS), Petropavlovsk-Kamchatsky
2. Institute of Volcanology and Seismology, RAS, Petropavlovsk-Kamchatsky
3. Institute of Earthquake Prediction Theory and Mathematical Geophysics of RAS, Moscow

### 1.2 The February 28, 2013, $M_W$ 6.8 South Kamchatka Earthquake

#### 1.2.1 Introduction

On February 28, 2013, at 14:05 (UTC) a magnitude  $M_W$  6.8 earthquake occurred near the South-East Coast of Kamchatka (Figure 1.1). The source is located in the Pacific Ocean, 120 km east of Severo-Kurilsk, and 270 km south of Petropavlovsk-Kamchatsky. Hypocenter parameters of the earthquake, its

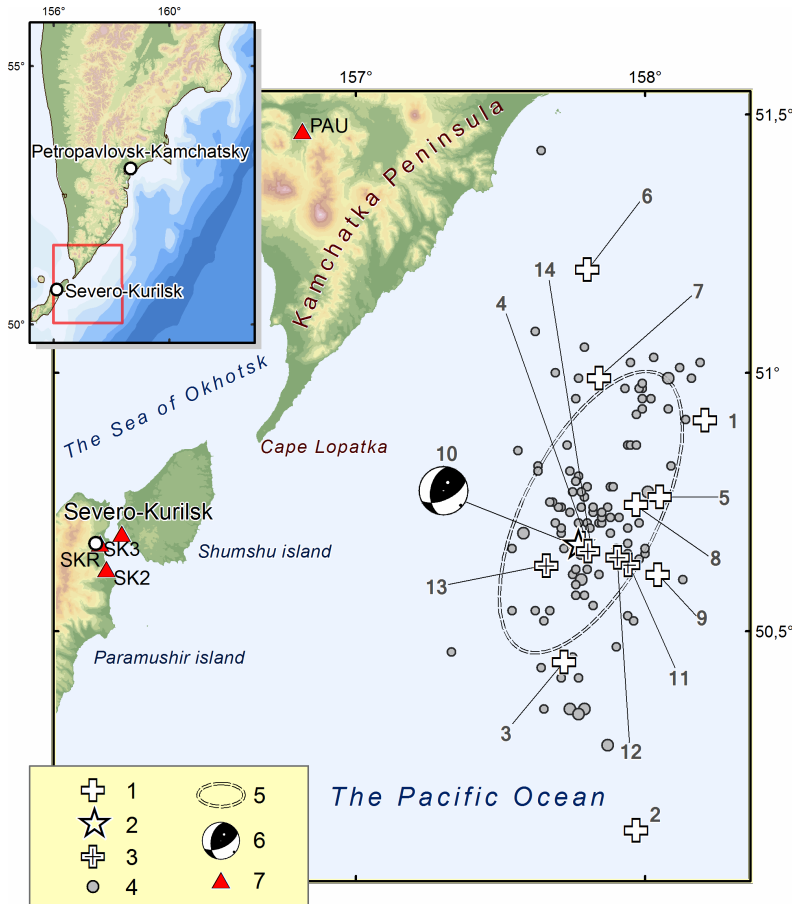


**Figure 1.1:** Location scheme for epicenters of the February 28, 2013 earthquake, its aftershocks with  $ML > 3.5$ , and strong earthquakes ( $ML > 6.0$ ) of this region for the period from 1962 to February 28, 2013, according to the catalogue of Kamchatka and the Commander Islands earthquakes ( $ML > 3.5$  corresponds to the catalogue completeness threshold for the Kamchatka regional network within area of responsibility). 1 - epicenters of strong earthquakes of this region for the period from 1962 to February 28, 2013; 2 - the epicenter of the February 28, 2013 earthquake; 3 - epicenters of strong aftershocks ( $ML > 6.0$ ); 4 - epicenters of aftershocks with  $3.5 \leq ML \leq 6.0$ ; 5 -  $2\sigma$ -ellipse approximation of the aftershock zone; 6 - stereogram of the focal mechanism by Global CMT for the main earthquake; 7 - seismic stations. Numeration of earthquakes corresponds to Table 1.1.

strong aftershocks with  $ML > 6.0$  and strong earthquakes ( $ML > 6.0$ ) of this area from 1962 to the main event of February 28, 2013 and their magnitude estimations according to several seismological agencies of Russia and the world are given in Table 1.1. According to the Kamchatka Branch of the Geophysical Survey of Russian Academy of Sciences (GS RAS) the earthquake intensities were reported to be up to V-VI on the Medvedev-Sponheuer-Karnik scale (MSK-64) (Medvedev *et al.*, 1965) in settlements on Kamchatka peninsula.

Real-time earthquake processing by Seismological Subsystem of Tsunami Warning System (SS TWS by KB GS RAS) was performed in accordance with accepted time limits. Earthquake alerts and hypocenter parameters were released three times, in 1, 4 and 6 minutes from the first arrival at the closest seismic station. The final SS TWS solution was: 14:05:50 (UTC); 50.89°N, 157.55°E, depth  $h = 61$  km,  $M_S = 6.4$ ,  $M_S(20R) = 6.6$ ,  $ML = 6.9$ . Tsunami alert was not issued. There were no tsunami waves registered by mareographs of Kamchatka Tsunami Warning Center of Roshydromet (Petropavlovsk-Kamchatsky).

The 65 strongest earthquakes final solutions have been published with a delay of no more than a day. In total, during the first 10 days there were 102 aftershocks registered with a magnitude of  $ML = 2.6-6.8$ . Final processing of the event sequence for the first 10 days was completed by March 10. Further events were processed in the normal mode with a delay of no more than a day.

№	Hypocenter					Energy class / Magnitudes								
	Date YYYY.MM DD.	Time hh:mm:ss	$\phi^\circ, N$	$\lambda^\circ, E$	h, km	KB GS RAS			Global CMT	NEIC(USGS)			Obninsk	
						$K^{F68}$	$ML$	$M_c$	$M_W$	$m_b$	$M_S$	$M_W$	$m_b$	$M_S$
Strong earthquakes of this area for the period from 1962 to February 28, 2013														
1	1966.04.08	01:46:43.4	50.91	158.21	18	13.9	6.2	-	-	6.0	-	-	-	-
2	1966.06.21	23:06:29.2	50.12	157.97	25	13.5	6.0	-	-	5.5	-	-	$M = 5$	
3	1973.03.12	19:39:19.6	50.44	157.72	39	14.3	6.4	-	-	6.1	-	-	6.0	6.2
4	1973.04.12	13:49:14.2	50.67	157.78	20	14.2	6.4	-	-	6.1	-	-	6.1	6.4
5	1992.07.13	15:34:03.3	50.76	158.05	39	13.7	6.1	-	6.1	5.7	5.8	6.2	5.8	5.9
6	1993.06.08	13:03:37.0	51.20	157.80	40	15.0	6.8	7.3	7.5	6.4	7.3	7.1	6.5	7.4
7	1999.09.18	21:28:34.2	50.99	157.84	40	13.8	6.2	6.0	6.0	5.9	5.6	6.0	6.2	5.6
8	2006.08.24	21:50:34.1	50.75	157.97	38	14.3	6.4	6.4	6.5	5.9	6.2	6.5	6.0	6.3
9	2008.07.24	01:43:15.8	50.61	158.04	40	13.8	6.2	6.1	6.2	6.0	6.0	6.2	6.1	6.1
The February 28, 2013 earthquake and its strong aftershocks														
10	2013.02.28	14:05:48	50.672	157.773	61	15.2	6.9	6.6	6.8	6.4	6.7	6.9	6.3	6.8
11	2013.03.01	12:53:49	50.628	157.941	52	14.2	6.4	5.9	6.4	5.7	5.8	6.4	5.8	6.4
12	2013.03.01	13:20:48	50.643	157.904	62	15.1	6.8	6.5	6.5	6.3	6.3	6.5	6.2	6.6
13	2013.03.04	20:56:33	50.627	157.658	51	13.6	6.1	5.1	5.3	5.3	4.8	0	5.4	4.7
14	2013.03.09	14:56:27	50.655	157.803	49	13.7	6.1	5.6	5.8	5.7	5.3	5.8	5.7	5.5

Note:  $K^{F68}$  - K-class magnitude of S-wave;  $ML$  - local magnitude;  $M_c$  - coda magnitude;  $M_W$  - moment magnitude;  $m_b$  - short-period body-wave magnitude;  $M_S$  - surface-wave magnitude.

**Table 1.1:** Parameters of strong earthquakes in the South Kamchatka region from 1962 to March 2013, including February 28, 2013 earthquake and its strongest aftershocks

## 1.2.2 Focal mechanism of the earthquake

Table 1.2 shows parameters and stereograms of focal mechanisms for the February 28, 2013 earthquake and its strongest aftershocks mentioned in Table 1.1 according to catalogues of Global CMT and KB GS RAS. (Estimates from KB GS RUS are determined by using the polarity of  $P$  wave onsets at regional stations). All the mechanisms are consistent with the tectonic condition of sub-horizontal compression in the NW-SE direction. For most mechanisms the flat plane dips under the Kamchatka peninsula, which corresponds to the geometry of the subduction zone.

## 1.2.3 Main features of the aftershocks process

The aftershock sequence of the February 28, 2013 earthquake ( $M_W = 6.8$ ) was selected from the preliminary catalogue using a method after Molchan and Dmitrieva (1991); the software was developed by V. B. Smirnov (Lomonosov Moscow State University). This data collection includes 254 earthquakes with magnitudes in the range of  $ML = 2.2-6.8$  where  $ML$  is calculated from  $K^{F68}$  as  $ML = K^{F68}/2 - 0.75$ , where  $K^{F68}$  is the K-class magnitude (Fedotov, 1972; Bormann, 2002). The cumulative frequency-magnitude plot (Figure 1.2) indicates a catalogue completeness threshold of  $ML_{min} = 3.3$  which corresponds to the left edge of the linear part of the plot. Based on this threshold 121 out of 254 earthquakes were obtained from the preliminary catalogue until the end of 2013 for further analysis.

In Figure 1.1 aftershocks are contoured by the dispersion ellipse containing 90% of the aftershocks for the first month after the main earthquake, allowing to estimate the size of the rupture area of the February 28, 2013 earthquake ( $M_W = 6.8$ ) as 90 km (length)  $\times$  40 km (width).

The frequency-magnitude plot shows a gap of  $\Delta M = 1.3$  between the largest aftershocks and the rest of the sequence (Figure 1.2). Such gaps can be observed between a main shock and the aftershocks. However, in this study the gap is observed between the group of the five strongest events (earthquakes

№	Date YYYY.MM .DD	Time hh:mm:ss	h, km	The axes of the principal stresses						Nodal planes						Agency	
				T		N		P		NP1			NP2				
				pl	azm	pl	azm	pl	azm	stk	dip	slip	stk	dip	slip		
10	2013.02.28	14:05:59	45	77	313	2	215	13	124	36	58	92	212	32	86	Global CMT	
		14:05:48	61	59	27	30	225	8	131	65	59	126	191	46	46	KB GS RAS	
11	2013.03.01	12:53:58	44	78	300	0	30	12	120	30	57	90	210	33	90	Global CMT	
		12:53:49	52	62	327	9	221	27	126	43	72	99	196	20	64	KB GS RAS	
12	2013.03.01	13:20:55	41	77	313	2	216	13	126	214	32	87	37	58	92	Global CMT	
		13:20:48	62	66	71	16	201	17	296	193	64	73	49	31	122	KB GS RAS	
13	2013.03.04	20:56:36	44	78	297	1	33	12	124	32	57	88	216	33	93	Global CMT	
		20:56:33	51	79	267	6	32	9	123	27	54	82	221	37	101	KB GS RAS	
14	2013.03.09	14:56:32	47	79	330	3	323	11	132	45	56	94	218	34	84	Global CMT	
		14:56:27	49	81	229	9	49	0	139	41	46	78	238	46	102	KB GS RAS	

**Table 1.2:** Parameters of focal mechanisms of the main earthquake and its aftershocks with  $ML \geq 6.0$  from Table 1.1 according to the Global CMT and KB GS RAS data

with magnitudes  $ML \geq 6.1$ , including the main event and 4 strongest aftershocks) and the remaining aftershocks sequence with magnitudes  $ML \leq 4.8$ . The only earthquake in the magnitude range of  $ML = 4.8-6.0$  occurred a month after the main event when the seismic process probably came out of the active phase. Thus, the observed sequence of earthquakes has features of both a swarm and an aftershock sequence with  $ML \leq 4.8$ .

Figure 1.3 shows the cumulative number of aftershocks over time in log-log scale.

Until the end of day 1 the trend is linear thus following Omori's Law with a decay exponent  $p=1$ . However, after two earthquakes on March 01, 2013 with  $M_W = 6.4$  and  $M_W = 6.5$ , the behaviour of the sequence changes dramatically, indicating new aftershock process initiated by these two earthquakes. In more detail, the following characteristic stages (Figure 1.3) can be distinguished:

1. Hyperbolic (standard Omori) stage with

$$\frac{dN}{dt} \sim \frac{1}{t} \tag{1.1}$$

, where  $N$  is the cumulative number of aftershocks and  $t$  is time, until the strongest aftershocks occur on March 01, 2013. The duration of this stage is  $\sim 23$  hours. In this stage, the catalogue completeness threshold is equal to  $ML = 3.3$ ;

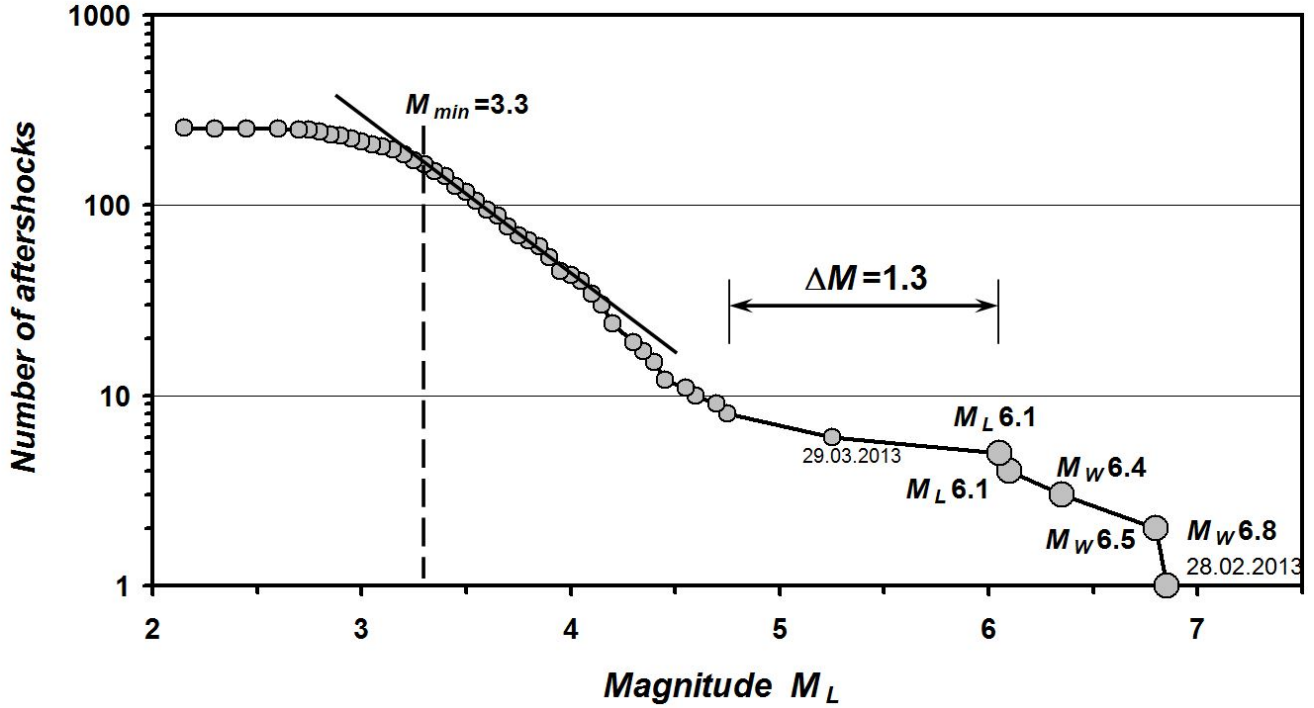


**Figure 1.2:** Cumulative frequency-magnitude plot for the aftershocks sequence of the February 28, 2013 earthquake ( $M_W = 6.8$ )

2. Strongest aftershocks occur on March 01, 2013 with  $M_W = 6.4$  and  $M_W = 6.5$ ; these are accompanied by decaying aftershocks following Omori's law

$$\frac{dN}{dt} \sim \frac{1}{t^p} \tag{1.2}$$

with  $p = 0.7$ . The duration of this stage is  $\sim 33$  hours. The catalogue completeness of the mode is equal  $ML = 3.3$ , except for the first 40 minutes;

3. The next stage showing a regular hyperbolic-law aftershock decay is the longest one, and lasts until June 2013. This date can be regarded as the end of the aftershock process that began with the earthquake on February 28, 2013,  $M_W = 6.8$ ; therefore total duration of the aftershock sequence can be estimated as  $\sim 100$  days. After this date, events in the area in question occur with intervals longer than one month.

### 1.2.4 Macroseismic data

Macroseismic information is collected for the 46 settlements of the Kamchatka region and the Northern Kuriles based on 109 reports of various sources. For the first time residents of the Kamchatka peninsula actively used an online questionnaire, which can be found on the official website of KB GS RAS (<http://www.emsd.ru/lspool/poll.php>). 59 respondents shared their experience from 9 locations. Although the earthquake occurred late at night on March 01, 2013 at 02:05 local time the online questionnaire system immediately began to receive reports from the respondents. By the beginning of the next working day the database of KB GS RAS already collected preliminary information about the intensity of ground shaking in 4 places: Petropavlovsk-Kamchatsky, Viluchinsk, Elizovo and Paratunka.

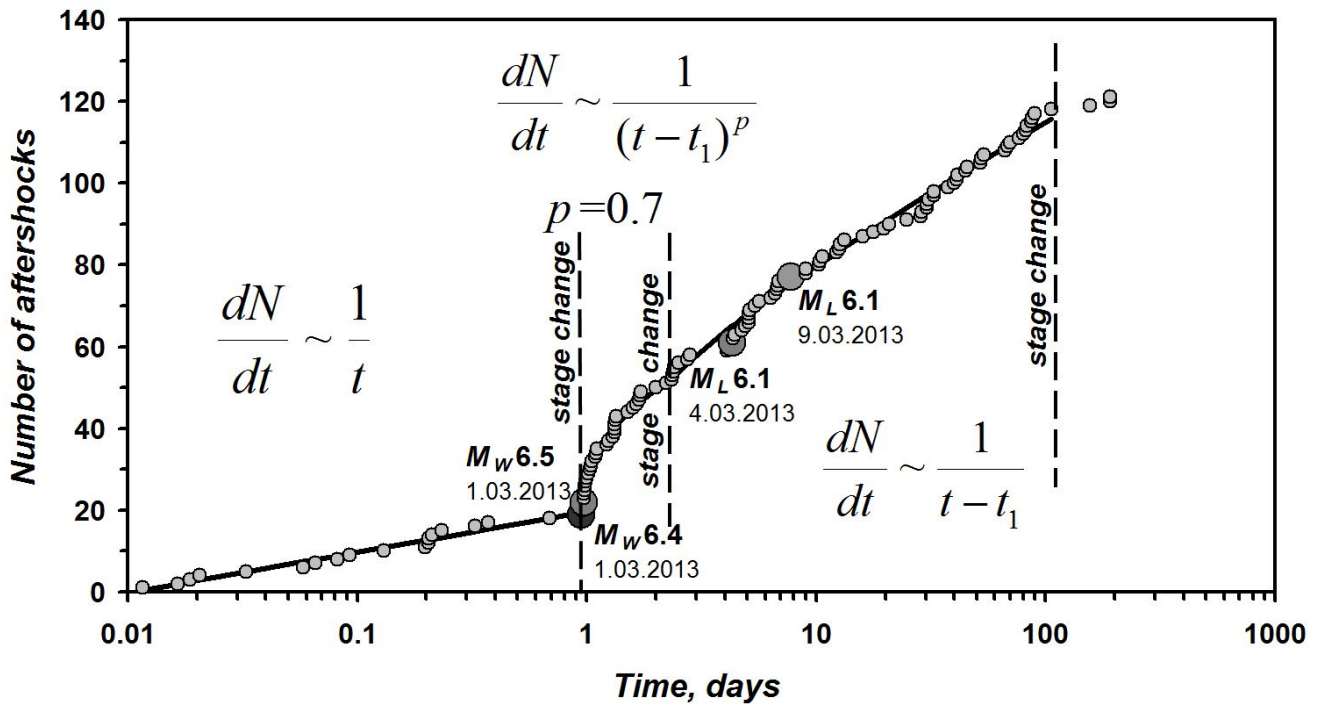


Figure 1.3: Development of the aftershock sequence with time. Origin time of the plot is set at the moment of the main shock on February 28, 2013 with  $M_W = 6.8$ , plus 0.01 day. The cumulative number of aftershocks is shown. The strongest earthquakes of the series are indicated.

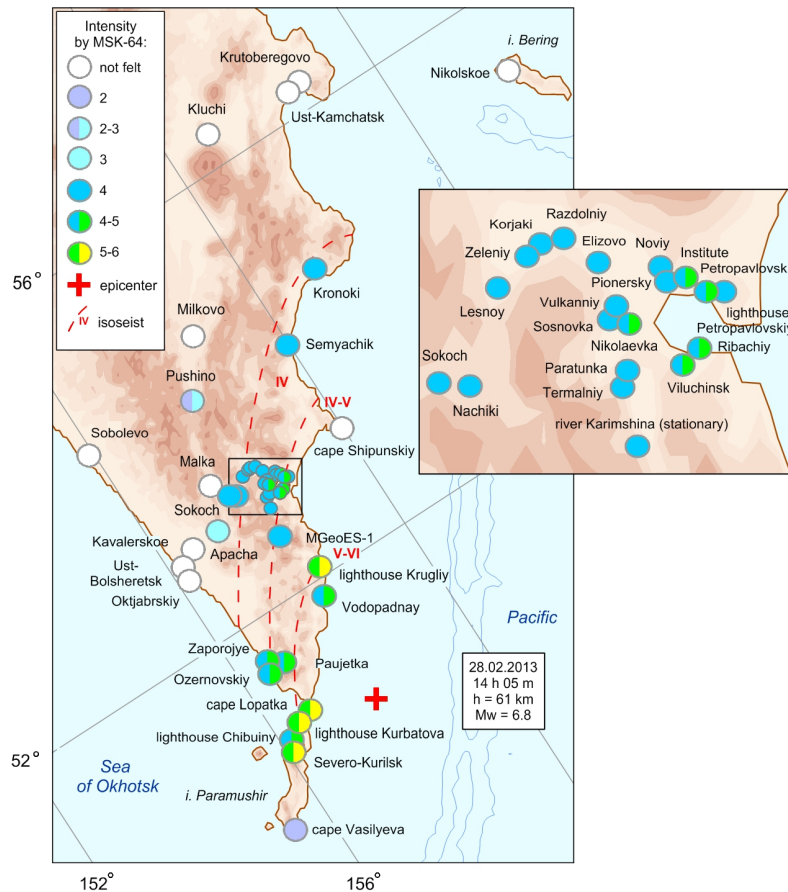
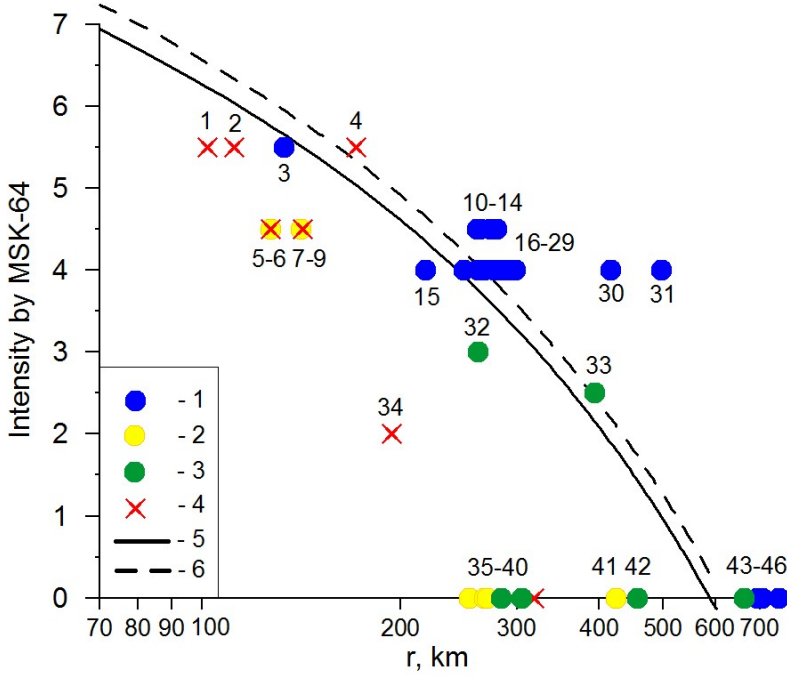


Figure 1.4: Macroseismic intensity distribution of the February 28, 2013 earthquake



**Figure 1.5:** Intensity ( $I$ ) decay with hypocentral distance ( $r$ ). 1 - observation sites located at the east coast of the Kamchatka Peninsula and Paramushir island; 2 - sites at the west coast; 3 - sites in central Kamchatka; 4 - sites with seismic intensity estimation from transmitted radiogram without text description (lighthouses and the Vodopadnaya meteorological station); 5, 6 - intensity decay curves calculated for  $M_W = 6.6$  and  $6.8$ , respectively, with Equation (1.3).

The earthquake was felt with intensities up to V-VI on the MSK-64 scale in 34 settlements located at epicentral distances from 82 to 492 km. The area of macroseismic effects is about 56 000 km<sup>2</sup>. A list of locations with epicentral distance, macroseismic intensity and effects description is given in Chebrov (2014).

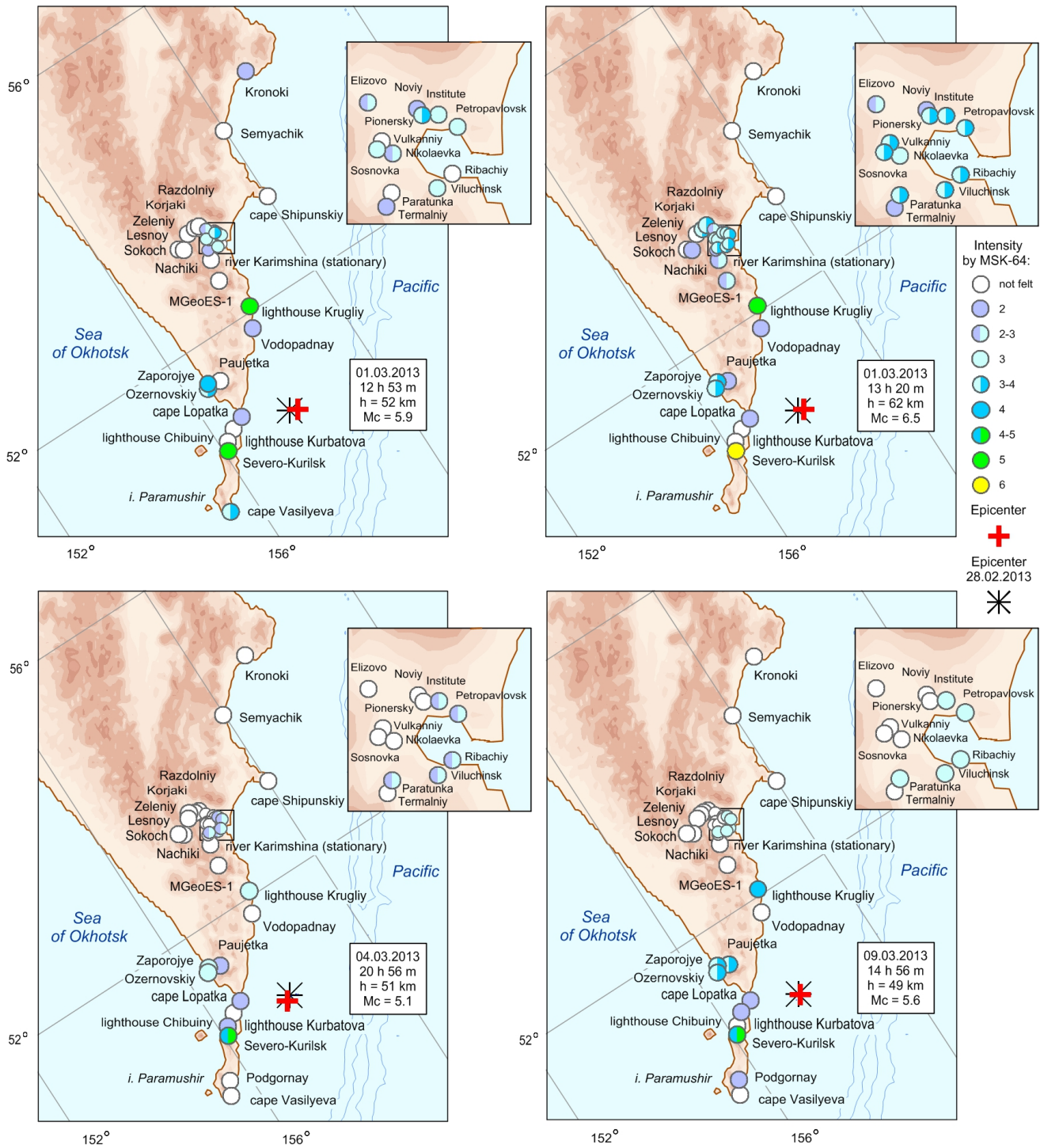
Figure 1.4 shows a map of isoseismals and reported intensities for the earthquake. Isoseismals are drawn schematically because of the small amount of data due to the lack of settlements in the study area. Isoseismals are elongated along the east coast of Kamchatka; this pattern is typical for Kamchatka earthquakes.

Figure 1.5 shows the reported intensities over hypocentral distance,  $I(r)$ , and theoretical decay curves of macroseismic intensity, calculated using the equation after Fedotov and Shumilina (1971):

$$I = 1.5 \cdot M - 2.63 \cdot \lg(r) - 0.0087 \cdot r + 2.5 \tag{1.3}$$

where  $I$  - macroseismic intensity;  $r$  - hypocentral distance;  $M$  - magnitude (In our calculations we used  $M_W$ ).

The macroseismic magnitude was estimated as  $M = 6.6$ ; this value was chosen as providing the best fit between intensity decay and observed data. In this fitting, the macroseismic earthquake hypocenter was assumed to coincide with the instrumental one. The graph shows that at equal distances from the hypocenter seismic intensity values in the settlements of the east coast are higher than values in central Kamchatka and the western coast where the earthquake was not felt at distances over 260 km. It should be noted that there is a lack of reported effects at Cape Shipunskiy (Figure 1.4), located on the east coast. Strong winds and storms often mask macroseismic effects at this site. Seismic intensities at the Vodopadnaya meteorological station, Chibuiny lighthouses, and Cape Vasilyeva are significantly lower than expected. This may be related to local site conditions, or due to a human bias of intensity values based on the reports of very small staff at the lighthouse.



**Figure 1.6:** Macroseismic effects of aftershocks of the February 28, 2013 earthquake, see also Table 1.1

After the February 28, 2013 earthquake four aftershocks with  $ML > 6.0$  (Table 1.1) occurred during the first 9 days and could be felt in Kamchatka (Figure 1.6). All events, including the main one, have a similar pattern in isoseismal maps: the macroseismic effect is higher on the eastern coast of Kamchatka with the strongest shaking recorded at Severo-Kurilsk on the Paramushir island (Figure 1.6).

### 1.2.5 Ground motion

Figure 1.7 illustrates the records of ground motion at the Severo-Kurilsk seismic station. Peak amplitudes for 29 stations are presented on Figure 1.8 (accelerations) and Figure 1.9 (velocities). When both accelerometer and velocimeter are present at a station, results recovered from records of both instruments are plotted.

There are sometimes significant discrepancies between the estimates of the amplitudes from an accelerometer and a velocimeter. This fact can result from various factors. At some stations the accelerometer is installed on a pedestal, usually in a building (single-storey), while the velocimeter is installed outside the building, at distances of  $\approx 40$  m, in a borehole at depths of 5-30 m. Additionally, instrument orientation azimuths for borehole instruments could bear large errors.

The decay of amplitudes with hypocentral distance  $r$  is analysed in the next paragraphs. Figure 1.8 shows the peak acceleration of the vertical and horizontal components with hypocentral distance. For comparison, two peak acceleration decay curves from other sources are plotted. Of the two parallel solid gray lines, the lower one is after Fukushima and Tanaka (1990) (with their epicentral distances converted to hypocentral ones). It follows the trend

$$A \sim r^{-1.218} \tag{1.4}$$

Its intersection with the y-axis corresponds to  $M_W = 7.0$ . The upper line is plotted through an anchor point at  $r = 200$  km using a point estimate derived from empirical scaling after Gusev *et al.* (1997). In that paper, only epicentral distances between 50-200 km were considered. Therefore, the line was plotted through the anchor point with the slope identical to that of Fukushima and Tanaka (1990). None of these approximations is acceptable. At distances above 300 km data points are below both straight lines. An alternative linear approximation of the data was found, based on the least squares method (dot-dashed line), with a slope of -2.55. Despite some improvement of the fit, the general agreement was still poor. As a final approximation we prefer three-segment broken line (dashes), with corner points at  $r = 300$  and 600 km, and slopes that vary, from left to right, from -1.37 to -2.42 and to -5.8.

In Figure 1.9, peak velocities are depicted. The reference straight line represents the calibration curve of the local K-class magnitude scale  $K^{F68}$  (Fedotov, 1972) with the standard slope of -1.75, and with its position along the y-axis selected for the best fit. This selection gives the corresponding magnitude value  $K^{F68} = 16.3$ . The peak velocity was estimated as  $2\pi (A/T)$  where A/T is the standard input of  $K^{F68}$  magnitude calculation. The actual value of  $K^{F68}$  for the main shock is 15.3, indicating amplitudes about 3.2 times lower than expected from the above estimate of  $K^{F68}=16.3$ . The discrepancy appears to be associated with significantly broader bandwidth of the digital velocimeter as compared to the emulated band-limited signal of 1.2s VEGIK seismograph channel used for the  $K^{F68}$  calculation. The qualitative agreement of the trend for observed data with the trend of the calibration curve is quite acceptable. It should be noted that the original calibration curve was constructed up to the 600 km distance; the success of its extrapolation up to 1600 km was unexpected.

A more detailed analysis of amplitudes can be carried out after careful classification of stations by their soil types. According to the analysis of limited data for amplitudes of the February 28, 2013 earthquake,

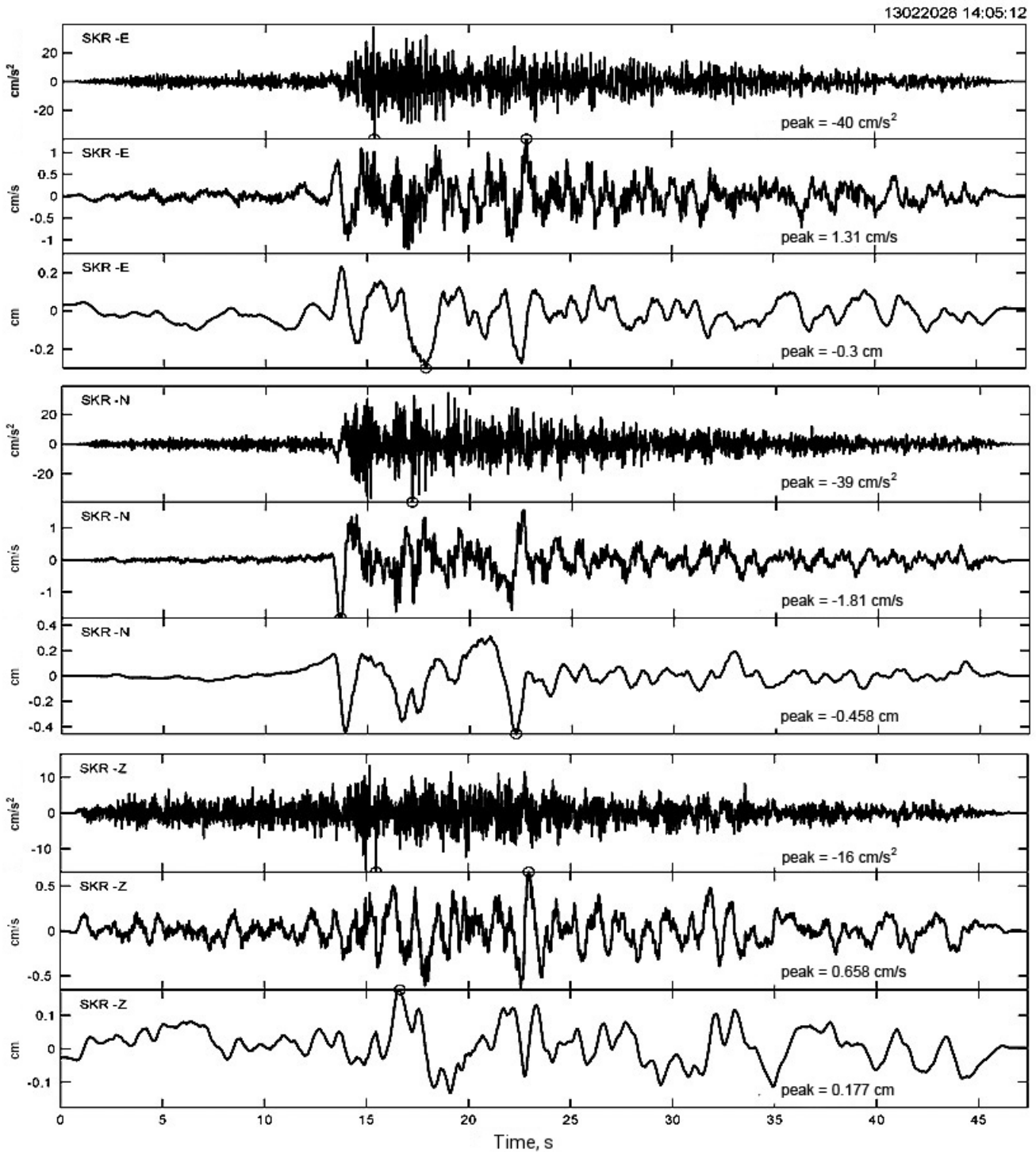


*Figure 1.7: Example of acceleration records at channels of digital Guralp CMG-5 accelerograph with the GEOSIG recorder at Severo-Kurilsk station (SKR), one of the closest to the epicenter, and recovered signals of velocity and displacement from these records in the frequency range from 0.1 to 40 Hz.*

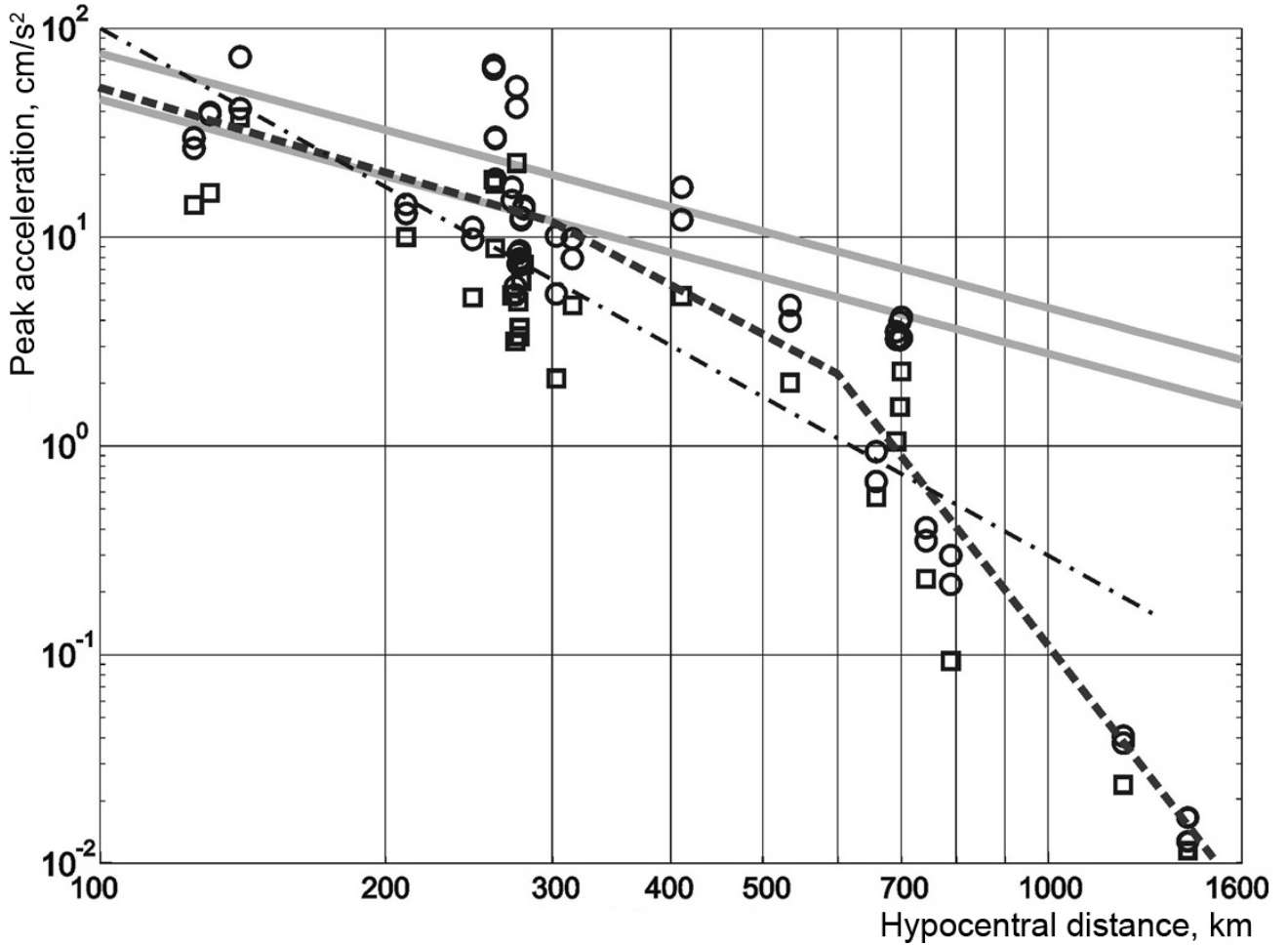


**Figure 1.8:** Peak acceleration with hypocentral distance. Circles and squares correspond to acceleration values on the horizontal and vertical components, respectively. Gray lines follow decay approximations based on Fukushima and Tanaka (1990) (lower) and Gusev et al. (1997) (top), for details see the text. Dot-dashed line shows a linear approximation of the data, which is not acceptable. The dashed line is the accepted 3-segment approximation.

preliminary conclusions can be made:

- (1) the level of acceleration and velocity amplitudes for the earthquake is approximately consistent with average tendencies for Kamchatka;
- (2) the distance decay for peak accelerations over the 100-300 km range is comparable to that for earthquakes of Kamchatka and Japan. The trend of  $A \sim r^{-1.218}$  is consistent with the data. At larger distances, the decay becomes much steeper.
- (3) the distance decay for peak velocities in the entire investigated distance range of 100-1600 km matches the calibration curve for regional K-class magnitude,  $K^{F68}$ , with its trend  $V \sim r^{-1.75}$ .

### 1.2.6 Conclusion

The February 28, 2013 earthquake of  $M_W = 6.8$  is a regular event in the seismic process of the Kuril-Kamchatka subduction zone. The earthquake occurred at the latitude of the Cape Lopatka. This segment of the Kuril-Kamchatka arc is one of the most seismically active areas in the North-West Pacific.

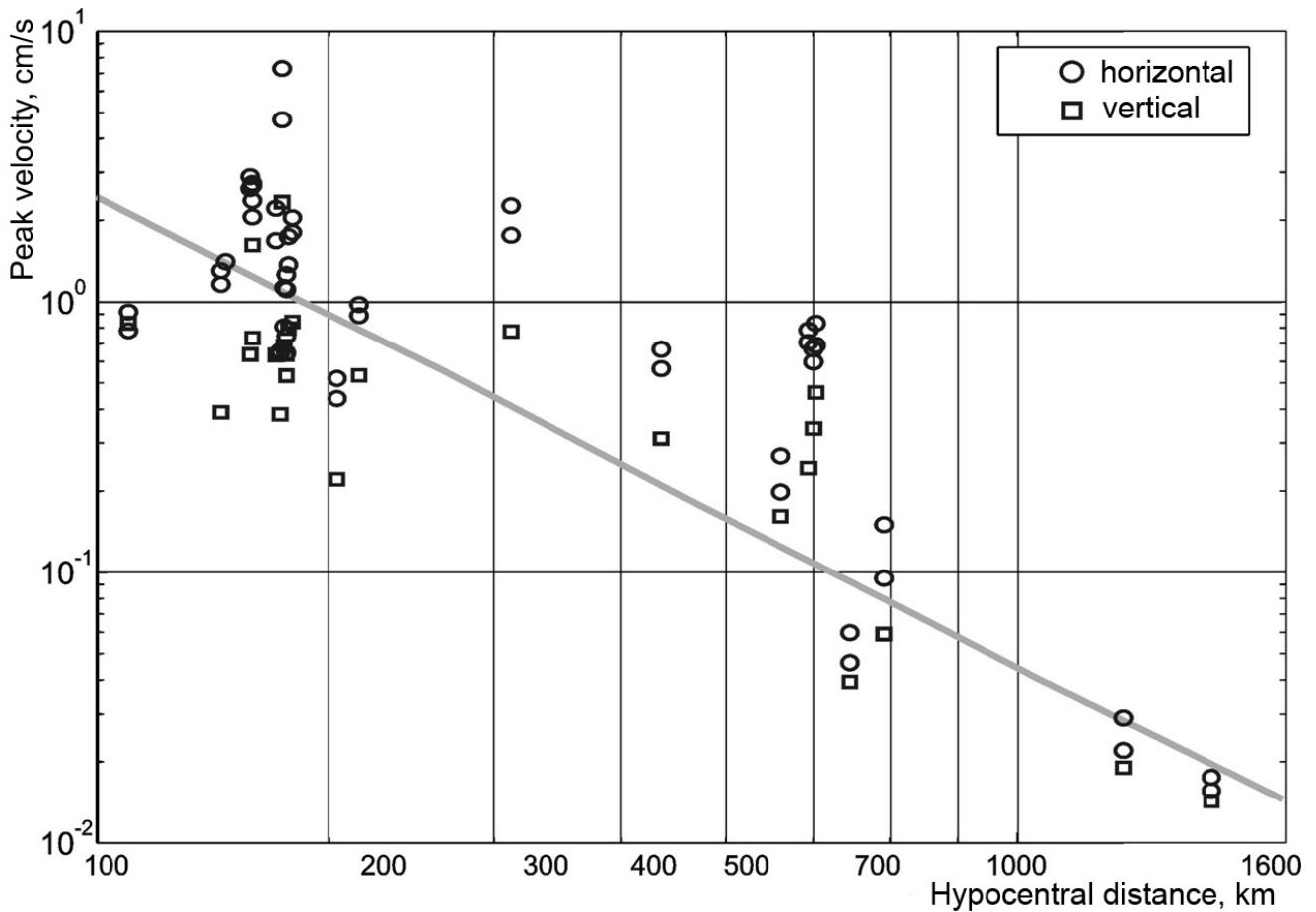


**Figure 1.9:** Peak velocities with hypocentral distance. The line shows the calibration curve of the Kamchatka  $K$ -class magnitude scale  $K^{F68}$  (Fedotov, 1972), with a value of  $K^{F68} = 16.3$ .

There have been repeatedly earthquakes with  $M > 8$  that caused tsunamis and intensities of ground shaking up to IX on the MSK-64 scale in the south of Kamchatka (Godzikovskaya 2010; Kondorskaya and Shebalin, 1977).

The last earthquakes with magnitudes of  $M \geq 7.0$  were recorded in the area of the North Kuriles in 1955 (on November 23, 1955,  $M = 7.3$  (Kondorskaya and Shebalin, 1977) and in 1973 (on February 28, 1973,  $M_W = 7.4$  (Gusev and Shumilina, 2004), and off the coast of south Kamchatka - in 1993 (on June 08, 1993,  $M_W = 7.5$  (Gusev and Shumilina, 2004) and in 1999 (on March 08, 1999,  $M_W = 6.9$ ). This area is located in an extensive fault zone that was ruptured by the strong catastrophic Kamchatka earthquake on April 11, 1952 with  $M_W = 9.0$  (Gusev and Shumilina, 2004), and probably lies in the fault zone of the first historical earthquake in Kamchatka on October 17, 1737 with  $M_W = 9.2$  (Gusev and Shumilina, 2004) described by S. P. Krasheninnikov (1949) and Godzikovskaya (2010) as well.

Parameters of the February 28, 2013 earthquake have been evaluated by SS TWS within 6 minutes, what is in accordance with accepted time limits. In urgent mode aftershocks have been processed. Macroseismic data have been collected for the region of Kamchatka and Northern Kuriles.

The actual time-magnitude pattern of the observed earthquake sequence is specific, with its properties between a standard aftershock sequence with a single mainshock, and a typical swarm with no main event. The aftershock cloud approximately covers an area of 90 km (length)  $\times$  40 km (width); these

figures provide a maximum estimate for the main shock fault size.

The analysis of peak accelerations shows typical amplitudes and decay within 250 km epicentral distance. At larger distances, a much stronger decay was revealed. The decay of peak amplitudes with epicentral distance matches the average trend for the Kamchatka region well. The February 28, 2013 earthquake of  $M_W = 6.8$  is the first earthquake of such magnitude in the Kamchatka region, that is recorded by the digital new system of seismic observations set by KB GS RAS between 2005 and 2010 (Chebrov *et al.*, 2013).

## 1.3 The largest deep-focus Sea of Okhotsk earthquake May 24, 2013, $M_W = 8.3$

### 1.3.1 Introduction

On May 24, 2013, at 05:44 (UTC) a magnitude  $M_W$  8.3 earthquake occurred in the Sea of Okhotsk, to the west of the Kamchatka Peninsula (Figure 1.10). The scalar seismic moment of the event is  $M_0 = 3.95 \cdot 10^{21} N \cdot m$  (Ekström *et al.*, 2012). This is the strongest earthquake recorded in the Kamchatka region during the years of instrumental seismological observations (from 1962 to present) and the most powerful earthquake in the world among events of comparable depths. A similar strong deep-focus event (647 km depth,  $M_0 = 2.63 \cdot 10^{21} Nm$ ) occurred in Bolivia, on June 9, 1994, but this event turned out to be weaker than the Sea of Okhotsk one.

Co-seismic displacement signals of the Sea of Okhotsk earthquake were recorded by many Far Eastern stations of the Global Navigation Satellite System (GNSS) (Chebrov *et al.*, 2013) and the macroseismic effect could be felt globally.

According to KB GS RAS, the epicenter of the May 24, 2013 earthquake is about 360 km north-west of Petropavlovsk-Kamchatsky, the hypocenter is located in the Kamchatka Benioff zone at a depth of 630 km, which corresponds to the lower depth limit for seismic events. The earthquake was followed by an aftershock sequence. Parameters of hypocenters for the earthquake and its strongest aftershocks with  $ML \geq 6.0$ , energy characteristics according to several seismological agencies of Russia and the world are given in Table 1.3.

Previous strong deep-focus earthquakes in the Sea of Okhotsk area occurred on July 05, 2008 at a depth of 665 km with  $M_W = 7.7$  and on November 24, 2008 at a depth of 564 km with  $M_W = 7.3$ .

The 2013 Sea of Okhotsk earthquake was felt in the Kamchatka region with intensities up to V-VI, and in the rest of Russia - up to IV-V degrees, as well as in several countries of Europe, Asia and North America. Macroseismic manifestations of the May 24, 2013 earthquake have been reported at epicentral distances up to 9500 km.

According to the SS TWS regulations real-time data processing started when an alarm signal was released (i.e. when the amplitude on a station exceeds the predetermined threshold value) after registering the P-wave onset at the "Karymshina" station (KRM). Processing was carried out within accepted time limits despite the strong ground shaking with intensities up to IV-V at the office's location. A preliminary assessment of source parameters was obtained within 4 minutes since the alarm, and a final one was released within 8 minutes since the alarm. All the relevant messages were sent according to the circulation list. The on-duty staff decided not to issue a tsunami alarm because the earthquake hypocenter was located at a depth greater than 600 km.

The reference magnitude to assess the tsunamigenic potential of an earthquake in the SS TWS is the surface-wave magnitude  $M_S$ . It should be noted that this magnitude has been underestimated in the preliminary solution ( $M_S = 6.7$ ). It is well known that deep earthquakes produce significantly reduced surface waves what leads to magnitude underestimation. Earthquake records are shown in Figure 1.11.

Thus, the earthquake processing time of SS TWS is about 8 minutes, which is within the approved

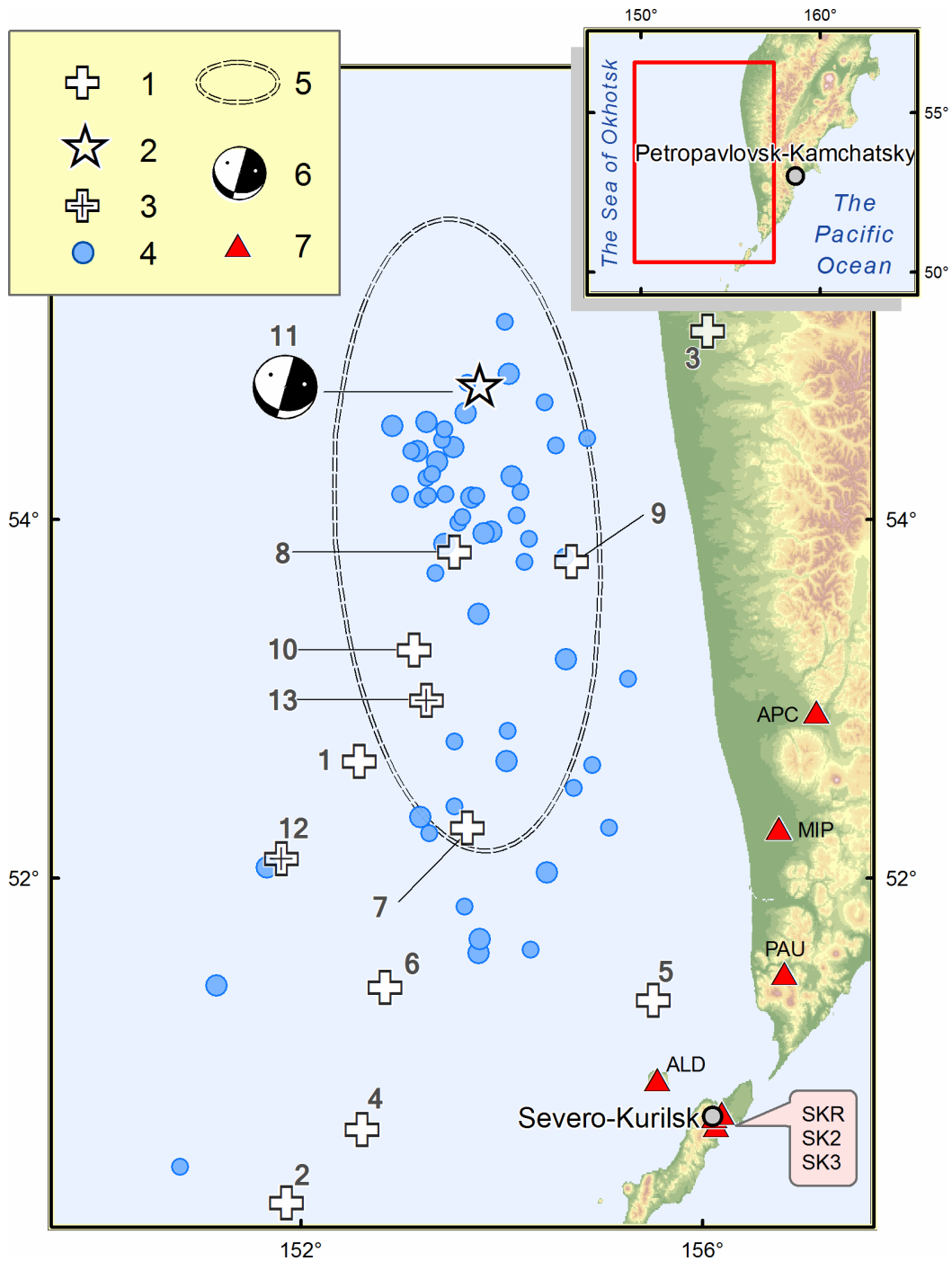


**Figure 1.10:** Location scheme for epicenters of the May 24, 2013 earthquake, its aftershocks with magnitudes of  $ML \geq 4.2$  and strong earthquakes ( $ML > 6.0$ ) of this region for the period from 1962 to May 24, 2013 according to the catalogue of Kamchatka and the Commander Islands earthquakes ( $ML \geq 4.2$  corresponds to the catalogue completeness threshold for the Kamchatka regional network in the Sea of Okhotsk region): 1 - epicenters of strong earthquakes ( $ML > 6.0$ ) of this region for the period from 1962 to May 24, 2013, 2 - the epicenter of the May 24, 2013 earthquake; 3 - epicenters of strong aftershocks ( $ML > 6.0$ ); 4 - epicenters of aftershocks with  $4.2 \leq ML \leq 6.0$ ; 5 -  $2\sigma$ -ellipse approximation of the aftershock zone; 6 - stereogram of the focal mechanism by Global CMT for the main shock; 7 - seismic stations. Numeration of earthquakes corresponds to Table 1.3.

№	Hypocenter					Energy class / Magnitudes							
	Date YYYY.MM DD.	Time hh:mm:ss	$\phi^\circ, N$	$\lambda^\circ, E$	h, km	KB GS RAS			Global CMT	NEIC(USGS)		Obninsk	
						$K^{P68}$	$M_L$	$M_c$	$M_W$	$m_b$	$M_W$	$m_b$	$M_S$
Strong earthquakes of this area for the period from 1962 to May 24, 2013													
1	1965.08.01	16:41:07	52.65	152.58	460	14.1	6.3	—	—	5.1	—	—	—
2	1971.01.29	21:57:51	50.19	151.86	710	15.2	7.3	—	—	6.1	—	6.8	—
3	1972.05.27	04:06:45	55.05	156.05	467	14.0	6.2	—	—	5.7	—	6.2	—
4	1975.12.21	10:54:06	50.60	152.61	701	15.2	6.8	—	—	6.0	—	6.4	—
5	1977.09.21	21:01:42	51.32	155.51	247	13.7	6.1	—	—	5.6	—	6.1	—
6	1979.12.30	04:18:21	51.39	152.84	682	13.6	6.0	—	—	5.4	—	5.8	5.0
7	2001.02.07	15:16:10	52.28	153.66	476	14.2	6.4	5.0	5.7	5.6	5.7	5.9	—
8	2008.07.05	02:12:06	53.82	153.53	610	15.7	7.1	6.9	7.7	6.8	7.7	6.9	6.5
9	2008.11.24	09:02:52	53.76	154.69	564	15.2	6.8	6.7	7.3	6.5	7.3	6.5	6.2
10	2009.12.10	02:30:51	53.40	152.61	621	14.8	6.6	5.4	6.3	6.1	6.3	6.2	—
The May 24, 2013 earthquake and its strongest aftershocks													
11	2013.05.24	05:44:47	54.76	153.79	630	17.0	7.8	7.4	8.3	7.5	8.3	7.7	—
12	2013.05.24	14:56:29	52.11	151.81	642	15.0	6.8	5.8	6.7	6.7	6.7	7.0	—
13	2013.10.01	03:38:19	52.99	153.25	605	15.2	6.9	6.1	6.7	—	—	6.7	—

Note:  $K^{P68}$  - K-class magnitude of S-wave;  $M_L$  - local magnitude;  $M_c$  - coda magnitude;  $M_W$  - moment magnitude;  $m_b$  - short-period body-wave magnitude;  $M_S$  - surface-wave magnitude.

**Table 1.3:** Parameters of strong earthquakes ( $M_L \geq 6.0$ ) in the Sea of Okhotsk region from 1962 to May 2013, including the May 24, 2013 earthquake and its strongest aftershocks

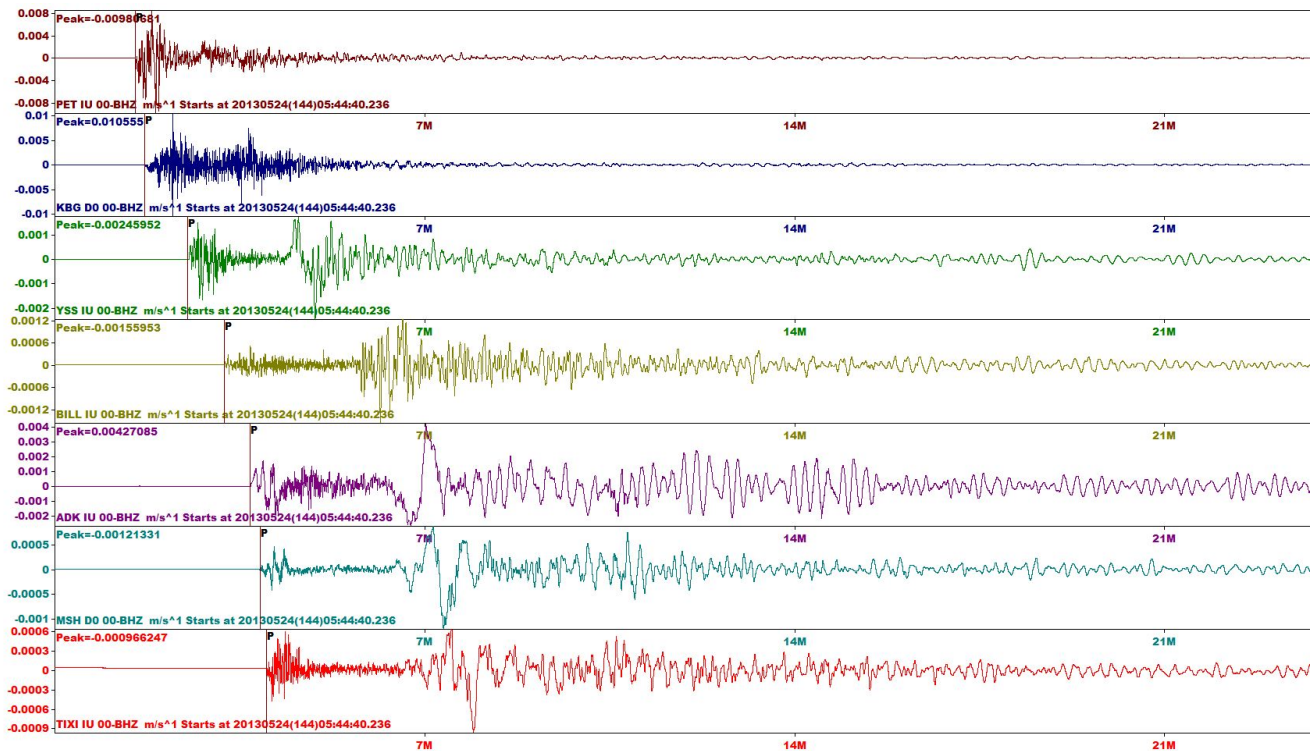


**Figure 1.11:** Examples of earthquake records of the May 24, 2013 earthquake at broadband seismic stations (vertical channels): PET - “Petropavlovsk”; KBG - “Krutoberegovo”; YSS - “Yuzhno-Sahalinsk”; BILL - “Bilibino”; ADK - “Adyak”; MSH - “Schultz Cape”; TIXI - “Tiksi”

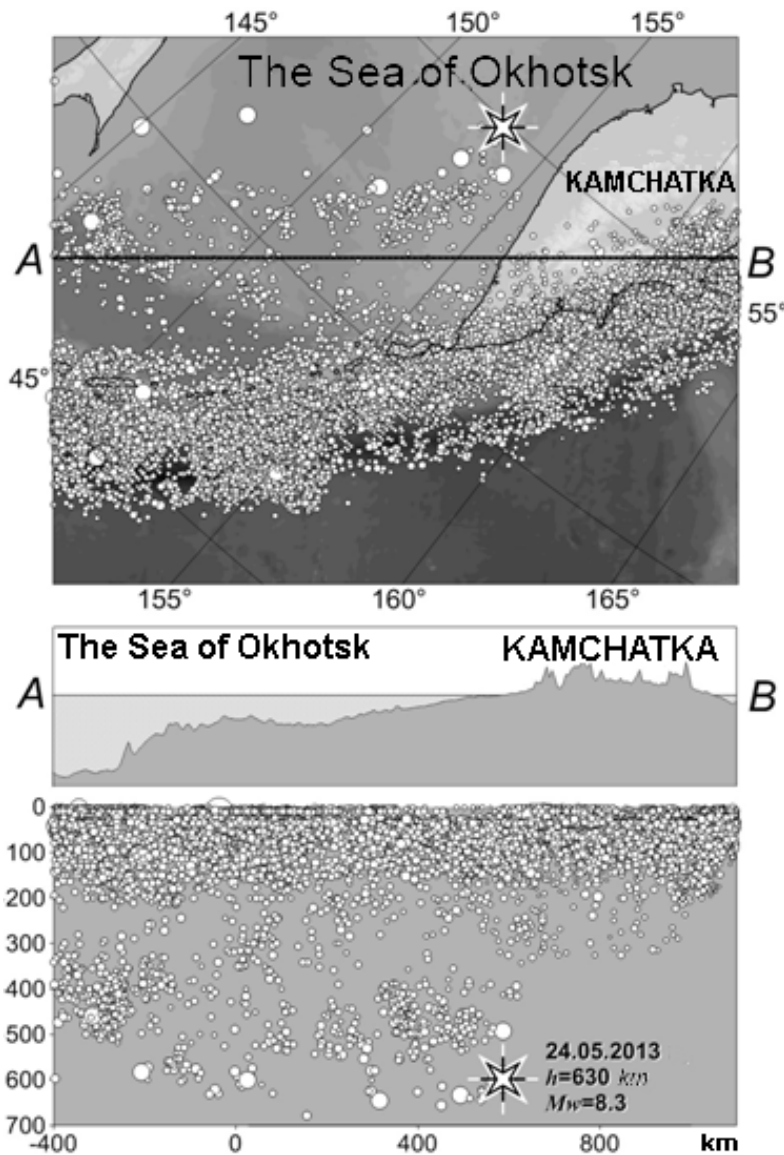


*Figure 1.12: Locations for the epicenters of the May 24, 2013 earthquake and other events of the focal zone from 1962 to August 2013 according to USGS NEIC PDE catalogue and the projection of its hypocenters on the vertical plane along a profile (AB)*

time limit (according to current regulations it should take not more than 10 minutes for processing earthquakes at epicentral distances of up to 1000 km). The processing centre "Petropavlovsk" in a challenging situation demonstrated sufficient accuracy in determination of earthquake parameters within their mission as an urgent service of tsunami warning system.

### 1.3.2 Tectonic setting and the focal mechanism of the earthquake

The Kuril-Kamchatka subduction zone can be divided along strike into two segments: the Kurile-South-Kamchatsky and the North-Kamchatsky segment (Levina *et al.*, 2013). The boundary between them is located in the Avacha Gulf area. Numerous geological and seismological data confirm the difference in ages of subduction on these two segments. The observed seismic focal zones are characterized in the southern and northern segments by fundamentally different depths, 650-700 km to the south and only 350-400 km to the north, respectively (Figure 1.12).

The deep-focus May 24, 2013 earthquake occurred almost at this boundary, or to be more specific at the north-eastern end of the Kuril-South-Kamchatka segment of the subducting Pacific plate. NE of the

epicenter, the depth position of the lower boundary of the Benioff zone moves up, from about 400 km at latitude 53.5N to about 120 km at 56N.

Focal mechanisms were determined using three types of data: (1) polarities of P waves; (2) co-seismic offsets at the GNSS stations (static case); and (3) waveforms registered at regional broadband seismic stations (dynamic case).

Parameters and stereograms of focal mechanisms for the May 24, 2013 earthquake and its strongest aftershocks with  $ML \geq 6.0$  according to catalogues of Global CMT and KB GS RAS (the latter estimates are determined using P wave polarities at regional and global stations) are given in Table 1.4. The most interesting fact is that all the solutions indicate compression down dip of the subducting Pacific plate.

№	Date YYYY.MM .DD	Time hh:mm:ss	h, km	The axes of the principal stresses						Nodal planes						Agency	
				T		N		P		NP1			NP2				
				pl	azm	pl	azm	pl	azm	stk	dip	slip	stk	dip	slip		
11	2013.05.24	05:45:08	611	34	102	1	192	56	283	12	79	-89	189	11	-93	Global CMT	
		05:44:47	630	39	81	28	196	39	311	196	90	62	106	28	180	KB GS RAS1)	
12	2013.05.24	14:56:34	642	19	124	11	30	68	272	25	64	-102	231	28	-67	Global CMT	
		14:56:29	642	9	138	9	229	78	3	56	55	-79	218	37	-105	KB GS RAS1)	
13	2013.10.01	03:38:24	585	13	171	28	74	59	284	59	64	-121	293	40	-44	Global CMT	
		03:38:19	605	25	190	21	90	56	325	83	73	-112	318	28	-39	KB GS RAS1)	

Note. 1) Input data are polarities of P-waves.

**Table 1.4:** Parameters of focal mechanisms of the May 24, 2013 earthquake and its strongest aftershocks with  $ML \geq 6.0$  from Table 1.3 according to the Global CMT and KB GS RAS data

The determination of focal mechanism in a general approach as a full seismic moment tensor (SMT) is described in Abubakirov *et al.* (2015), where six SMT components are calculated. The seismic moment tensor was determined using either co-seismic static offsets or waveforms (displacements) by a least-square linear inversion providing error estimations for each of the SMT components as standard deviations. Then the SMT eigenvalues and corresponding principal axes were estimated which allowed to determine (1) the best double couple (DC), (2) scalar seismic moment,  $M_0 = (E_3 - E_1)/2$ , and (3) Lode-Nadai coefficient,  $\eta = (2E_2 - E_1 - E_3)/(E_3 - E_1)$ , where  $E_1 \leq E_2 \leq E_3$  are SMT eigenvalues. The  $\eta$  value varies from -1 to 1 ( $\eta = 0$  corresponds to the pure double-couple source) and characterizes a discrepancy between a SMT solution and a DC.

In addition to the SMT, in the dynamic case the source is characterized by its source time function (STF), which describes the slip rate. In this study we assume the STF to be an isosceles triangle of unit area and the source epicenter is known from USGS PDE catalogue. The duration of the STF and the source depth are found by best fit during the inversion process.

All calculated variables are accompanied by error estimates. For variables that are functions of SMT

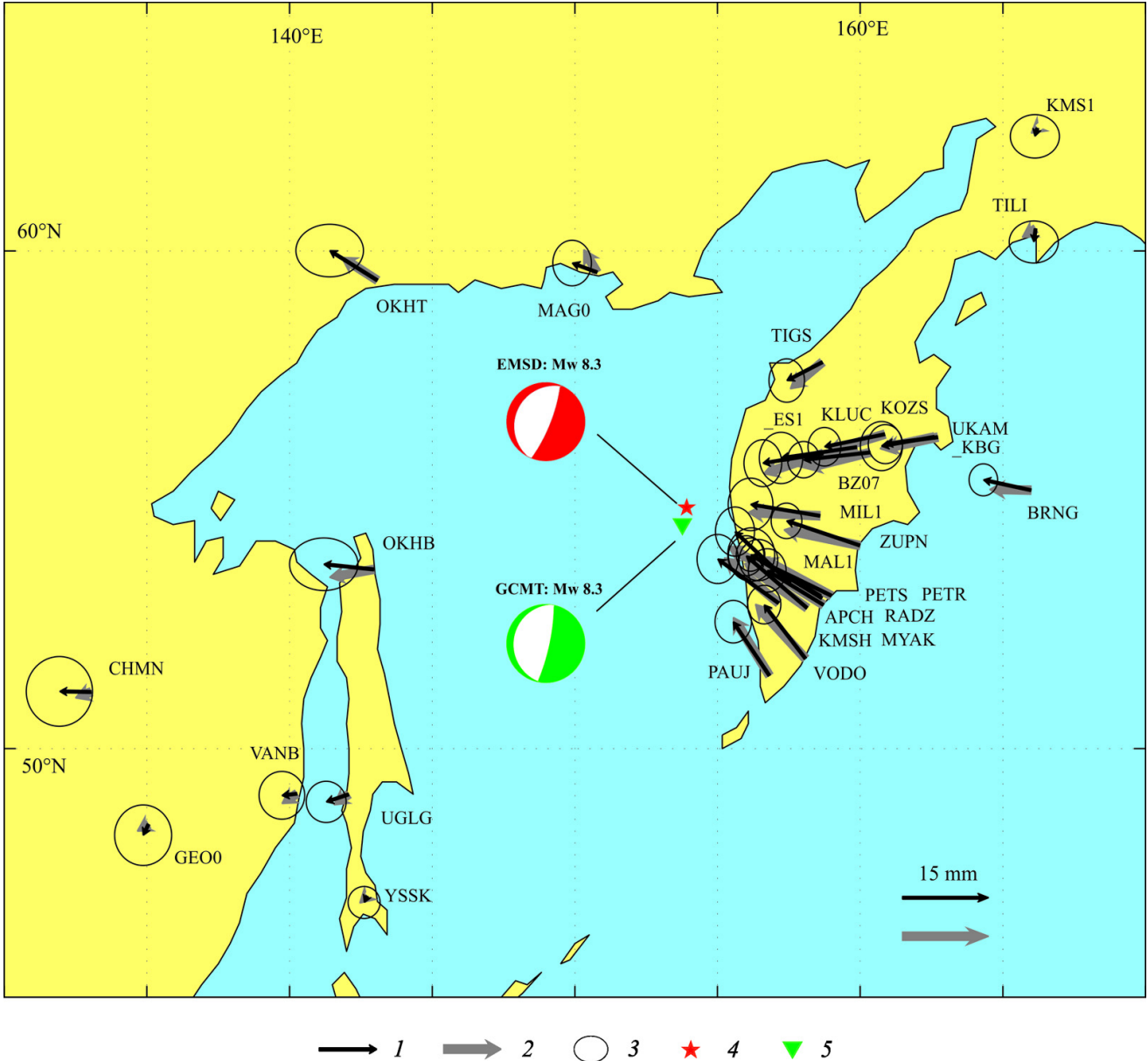


**Figure 1.13:** Horizontal components of observed offsets and simulated static displacements for the *ES\_1* option (parameters used for calculation are given in Table 1.5). 1 - observed horizontal offsets; 2 - simulated static offsets; 3 - error ellipses; 4 - epicenter as located by the KB GS (EMSD); 5 - epicenter according to the GCMT

components error estimates are obtained by the Monte-Carlo method. Namely, each optimal SMT component is disturbed by random normally distributed quantities with zero mean and standard deviation obtained by the LS inversion. For  $N$  realizations ( $N = 1000$ ) of the SMT, the set of values of a dependent scalar quality, say the largest eigenvalue, is generated. The estimate for such scalar quantity is the half-width of the interval (centered at the undisturbed value) that contains 68% of the points. Note that if a data distribution is normal then 68% of the data values are within one standard deviation of the mean. When we deal with a vector, we find half the angle at the vertex of a circular cone that contains 68% of the vectors based on the disturbed tensors. The axis of the cone is determined by the undisturbed vector.

For the static case we used three-component data from GNSS observations carried out by KB GS

RAS and networks of other institutions of the Far Eastern Branch of the Russian Academy of Sciences (Figure 1.13 shows horizontal offsets vectors). We assume that the source is a point source and located at the GCMT centroid. For SMT inversion we used the functions of influence of the SMT components or partial derivatives of Green’s functions with respect of source spatial coordinates. The influence functions - synthetic static displacements from unit couple corresponding to each of SMT component - were calculated for a layered sphere using an original algorithm (Abubakirov *et al.*, 2015).

For the dynamic case we used seismic broadband seismograms (Figure 1.14). Four seismic networks were used for processing: GSN (global seismic network), Japanese F-net network, Alaska Regional Network and China National Seismic Network. Additionally, we used reference stations of SS TWS by KB GS RAS and Tsunami Warning Center of USA West Coast and Alaska (West Coast & Alaska Tsunami Warning Center). For the SMT inversion we used records of stations with a low-frequency corner in the velocity transfer function at frequencies less than 8.33 mHz (period of at least 120 s). This condition allows us to reconstruct long-period ground motion with a sufficient enough signal-noise ratio.

The algorithm of dynamic inversion is presented in Pavlov and Abubakirov (2012). The functions of influence for the dynamic case were calculated for a layered half-space using the algorithm described in Pavlov (2013).

Seismic stations were selected in the epicentral distances of 8-25°. The upper limit of this range is set to ensure the applicability of the flat layered model of media used for the inversion, and the lower one is to ensure far-field conditions as calculations are based on a point-source model.

Calculation cases are described in Table 1.5. Besides the input data type (static or dynamic), they vary by number of components used and/or the number of unknown SMT components.

Used paramters	ES_1	ES14	ES35	ES25	ES35	ES36
Input data	Co-seismic offsets	Co-seismic offsets	Co-seismic offsets	Co-seismic offsets	Wave forms <sup>1)</sup>	Wave forms <sup>2)</sup>
Method of static offsets evaluation	1-1 <sup>3)</sup>	14-14 <sup>4)</sup>	14-14 <sup>4)</sup>	14-14 <sup>4)</sup>	-	-
Number of SMT components	3	3	3	2 <sup>5)</sup>	3	3
Number of unknowns	6	6	5 <sup>6)</sup>	5	5	6

Note.

- 1) In the interval  $[t_P, t_P + 900]$  s;
- 2) in the interval  $[t_P, t_S]$  s;
- 3) difference of observations after and before the earthquake;
- 4) difference of observations based on linear interpolations of data for 2 weeks after and 2 weeks before the earthquake;
- 5) horizontal components only;
- 6) SMT is assumed to have zero trace ( $M_{11} + M_{22} + M_{33} = 0$ ).

**Table 1.5:** Codes of calculation cases

The inversion results (Table 1.6, Table 1.7 and Figure 1.15) are compared to three SMT solutions available on the website of the USGS. All of these cases use the same condition (SMT is assumed to have zero trace). In the tables SMT solutions are coded as follows:

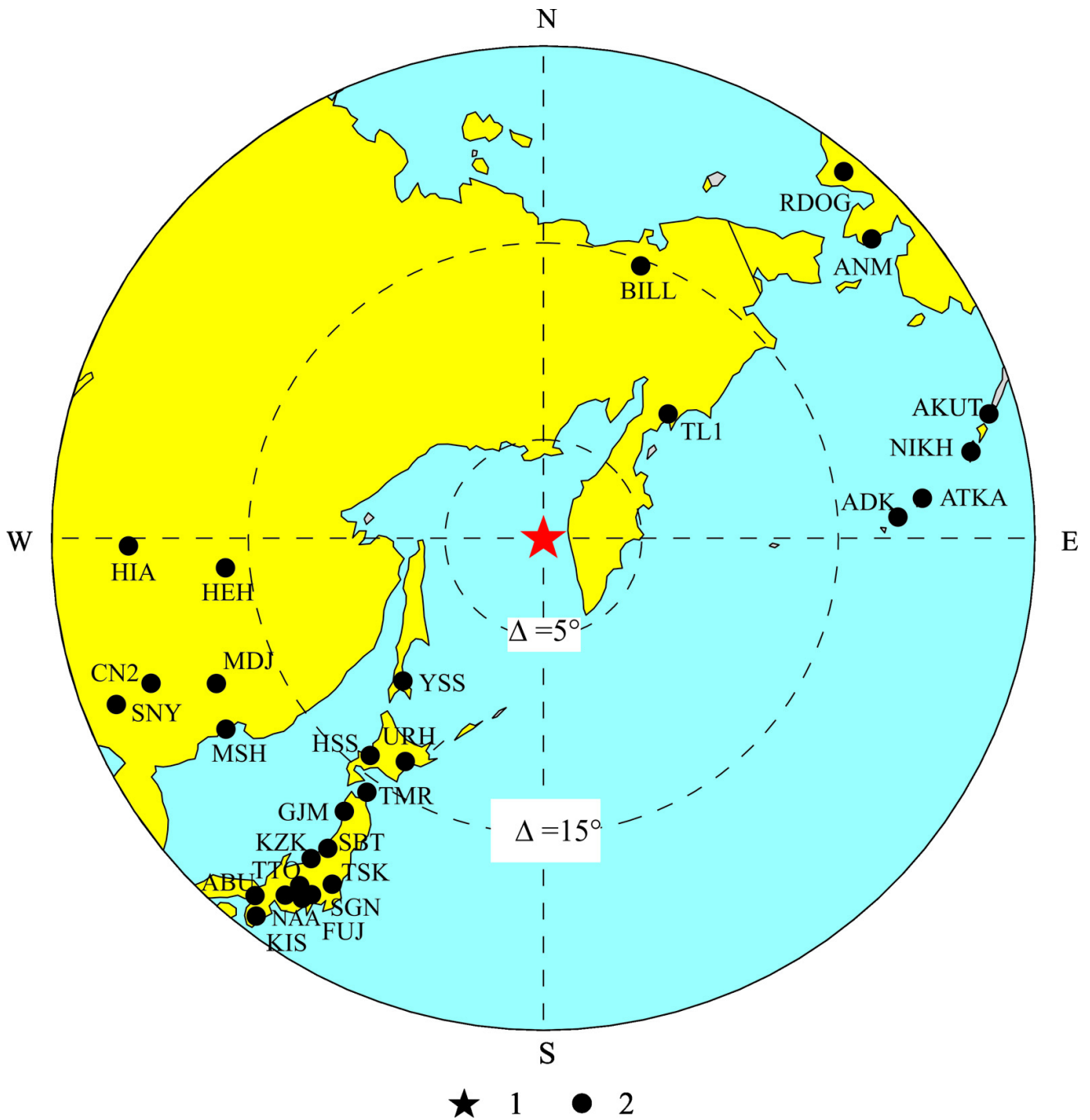


**Figure 1.14:** The location of instrumental epicenter by USGS (Table 1.4), the Sea of Okhotsk earthquake on May 24, 2013 (1) and used seismic stations (2)

Code	$M_{11}$	$M_{12}$	$M_{13}$	$M_{22}$	$M_{23}$	$M_{33}$	$\xi$	$\varepsilon, \%$
	$10^{21} N \cdot m$							
GCMT <sup>1)</sup>	1.28 $\pm 0.01$	-0.16 $\pm 0.01$	-3.57 $\pm 0.01$	0.38 $\pm 0.01$	0.78 $\pm 0.01$	-1.67 $\pm 0.01$	-	-
ES_1	1.11 $\pm 0.91$	-0.52 $\pm 0.36$	-3.37 $\pm 0.24$	0.27 $\pm 1.19$	1.29 $\pm 0.19$	-2.48 $\pm 0.46$	-0.37 $\pm 0.52$	2.6
ES14	1.41 $\pm 0.96$	-0.66 $\pm 0.39$	-3.71 $\pm 0.24$	1.86 $\pm 1.34$	1.46 $\pm 0.21$	-0.85 $\pm 0.51$	0.81 $\pm 0.57$	3.7
ES35	0.57 $\pm 0.42$	-0.51 $\pm 0.36$	-3.74 $\pm 0.24$	0.62 $\pm 0.44$	1.47 $\pm 0.21$	-1.19 -	-	3.8
ES25	0.58 $\pm 0.42$	-0.59 $\pm 0.35$	-3.84 $\pm 0.24$	0.57 $\pm 0.44$	1.60 $\pm 0.22$	-1.15 -	-	2.6
ED35	0.87 $\pm 0.07$	-0.06 $\pm 0.07$	-3.77 $\pm 0.09$	0.41 $\pm 0.07$	1.13 $\pm 0.07$	-1.29 -	-	20.8
ED36	0.62 $\pm 0.20$	-0.22 $\pm 0.22$	-5.06 $\pm 0.37$	0.46 $\pm 0.28$	1.52 $\pm 0.33$	-1.24 $\pm 0.60$	-0.06 $\pm 0.23$	20.8

Note. 1) It is given in full format (rounded) from GCMT catalogue (rounded).

**Table 1.6:** CMT-components  $M_{ij}$ , values of isotropic part  $\xi$  and residuals  $\varepsilon$

USGSW - The W-phase is used as raw data (seismogram segments from direct P wave to surface wave onsets) at regional and teleseismic distances, with filtering in a period range of 100-1000 s;

GCMT - the global catalogue of centroids and moment tensors. For calculations broadband seismograms are used at epicentral distances of  $\sim 30^\circ$  to  $\sim 90^\circ$ . In this case, the body waves are used (with periods of  $> 50$  s) and the mantle waves (with periods of  $> 200$  s);

USGSC - a version of CMT by National Information Center (NEIC) of US Geological Survey. Medium- and long-period body and surface waves were used for the calculations.

Table 1.6 shows the SMT components obtained by inversions and error estimates by the least-squares method. For cases of USGSW and USGSC error estimates are not provided. Also this table shows the values of the isotropic part of the SMT, if it is not assumed to be equal to zero. Table 1.7 shows such calculated variables as: SMT eigenvalues, strike, dip, slip, scalar seismic moment  $M_0$  for the best double couple (DC), discrepancy between SMT solution from DC -  $\eta$ , and also the value of moment magnitude  $M_W$ . All these values are given with error estimates. For cases of USGSW and USGSC error estimates are not available.

The duration of rupture process was estimated as 32 seconds. The calculation also gives an independent estimate of the depth,  $h = 640$  km, which allowed to estimate the error of about  $\pm 50$  km. This estimate is consistent with other definitions given in Table 1.4. The duration value is consistent with the independent evaluation of  $\sim 30$  s from the work of Ye *et al.* (2013). The value of the duration in the GCMT catalogue is  $\tau = 71.4$  s, which is more than double our estimate. However, the GCMT estimate is not a result of direct fitting, but assigned by the magnitude using a correlation equation (Ekström *et al.*, 2012).

For the ES\_1 case (using co-seismic offsets, details are in Table 1.5) Figure 1.15 shows the focal mechanism, cones, characterizing error estimates, eigenvectors positions and the neutral axis and quantities

Code	Eigenvalues, $10^{21} N \cdot m$			Focal mechanism			$\eta$ , %	$M_0$ $10^{21}$ $N \cdot m$	$M_W$
	$E_1$	$E_2$	$E_3$	Planes <sup>1)</sup>		Rake <sup>2)</sup>			
				$\varphi$ (°)	$\delta$ (°)	$\lambda_s$ (°)			
USGSW <sup>3)</sup>	-4.00	0.31	3.67	12/184	81/10	-89/-98	12	3.84	8.3
GCMT	-4.13 $\pm 0.01$	0.36 $\pm 0.01$	3.76 $\pm 0.01$	12/189 $\pm 0.1/1$	79/11 $\pm 0.1$	-89/-93 $\pm 0.2/1$	$14 \pm 0.3$	3.96 $\pm 0.01$	8.331 $\pm 0.001$
USGSC <sup>4)</sup>	-4.58	0.40	4.18	15/177	81/10	-87/-107	14	4.40	8.4
ES_1	-4.65 $\pm 0.45$	0.02 $\pm 1.0$	3.52 $\pm 0.66$	22/207 $\pm 4/33$	76/14 $\pm 3/4$	-91/-84 $\pm 8/29$	$14 \pm 24$	4.09 $\pm 0.31$	8.34 $\pm 0.02$
ES14	-3.71 $\pm 0.51$	1.30 $\pm 1.07$	4.84 $\pm 0.67$	25/246 $\pm 5/33$	80/13 $\pm 4/5$	-98/-50 $\pm 9/27$	$17 \pm 22$	4.27 $\pm 0.31$	8.35 $\pm 0.02$
ES35	-4.30 $\pm 0.37$	0.25 $\pm 0.44$	4.05 $\pm 0.31$	23/238 $\pm 3/26$	83/9 $\pm 3/4$	-95/-55 $\pm 5/26$	$9 \pm 16$	4.17 $\pm 0.26$	8.35 $\pm 0.02$
ES25	-4.39 $\pm 0.36$	0.14 $\pm 0.44$	4.25 $\pm 0.32$	24/240 $\pm 3/25$	83/9 $\pm 3/4$	-95/-53 $\pm 4/25$	$5 \pm 15$	4.32 $\pm 0.26$	8.36 $\pm 0.02$
ED35	-4.29 $\pm 0.09$	0.42 $\pm 0.07$	3.87 $\pm 0.09$	16/188 $\pm 1/7$	82/8 $\pm 1/1$	-89/-98 $\pm 1/7$	$15 \pm 3$	4.08 $\pm 0.08$	8.34 $\pm 0.01$
ED36	-5.64 $\pm 0.51$	0.35 $\pm 0.29$	5.12 $\pm 0.45$	17/213 $\pm 4/22$	85/5 $\pm 2/2$	-91/-74 $\pm 2/22$	$11 \pm 8$	5.38 $\pm 0.37$	8.42 $\pm 0.02$

Note.

1) The plane orientation is defined by two angles - the strike  $\varphi$  and dip  $\delta$  (angle for the second plane is given after the slash);

2) rake  $\lambda_s$  - the angle in the focal plane between the strike direction and the slip vector (measured anti clockwise from the strike direction);

3) obtained by W-phase

([http://earthquake.usgs.gov/earthquakes/eventpage/usb000h4jh#moment-tensor?source=us&code=usb000h4jh\\_Mww](http://earthquake.usgs.gov/earthquakes/eventpage/usb000h4jh#moment-tensor?source=us&code=usb000h4jh_Mww));

4) CMT obtained by USGS NEIC

([http://earthquake.usgs.gov/earthquakes/eventpage/usb000h4jh#moment-tensor?source=us&code=pde20130524054448980\\_598\\_C\\_UCMT](http://earthquake.usgs.gov/earthquakes/eventpage/usb000h4jh#moment-tensor?source=us&code=pde20130524054448980_598_C_UCMT))

**Table 1.7:** Parameters of the Sea of Okhotsk earthquake: eigenvalues, mechanism, discrepancy between SMT solution and double couple  $\eta$ , scalar seismic moment  $M_0$ , and moment magnitude  $M_W$

for other cases of this study and those obtained by other agencies. All cases show similar solutions.

The  $M_0$  values for all the cases are consistent. The only exception is the ED36 dynamic case. Input data used for ED36 (excluding S waves) are not sufficient enough.

Using seismological data parameters of the finite source, such as rupture velocity ( $V_r$ ), duration time, rupture area were estimated by Ye *et al.* (2013). They found that the radiated seismic energy  $E_R$  is  $E_R = 1.5 \times 10^{17}$  J, rupture velocity is  $V_r = 4$  km/s, and average stress drop is  $\Delta\sigma = 15$  MPa. The estimated slip distribution along the fault plane is heterogeneous, with an average slip of 1.9-2.3 m, and a maximum slip of 9.9 m. The rupture area is  $180 \times 60$  km.

Another interpretation of GNSS data for the Sea of Okhotsk earthquake in terms of a dislocation model are described in Steblov *et al.* (2014) and Shestakov *et al.* (2014), using the shallow dipping plane of the GCMT focal mechanism. Shestakov's input data set is similar to ours; Steblov's data set is not as dense for the Kamchatka part as the other two sets, but includes additional GNSS stations in the Kuril Islands. All three working groups use different methods to determine static offsets from raw data.

The individual determination of such values as fault area (A) and slip (D), instead of  $A \cdot D$ , is a challenging

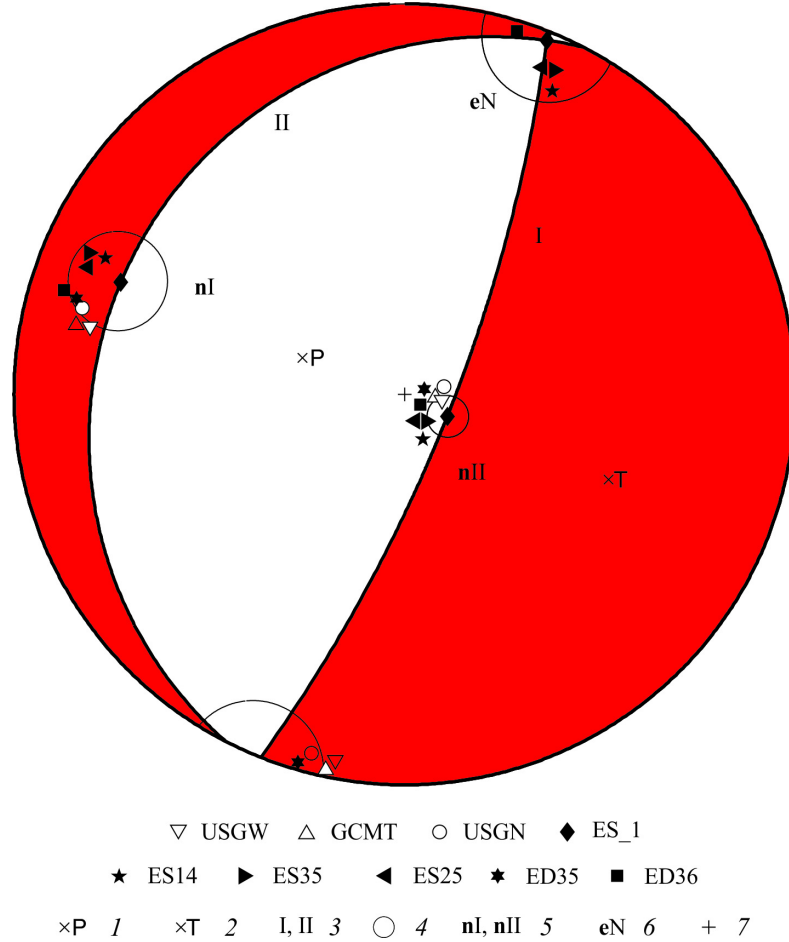


**Figure 1.15:** The mechanism for *ES\_1* case on a stereogram of the lower hemisphere. 1, 2 - axis of stress and strain; 3 - nodal planes; 4 - projection of the part of focal sphere that belongs to a cone reflecting error estimates; eigenvectors position (5) and the neutral axis (6) for all the cases from Table 1.7; 7 - the center of projection. The value of the half-angle of the axial section of the cone equals to  $6^\circ$  for the cone at *nI*,  $9^\circ$  - at *nII* and  $10^\circ$  - at *eN*

task as mentioned in Steblov *et al.* (2014). When the second plane, instead of the preferred one, of the GCMT focal mechanism is used for inversion, a similar misfit is found (Shestakov *et al.*, 2014). In general, observed data are not sufficient to distinguish the true plane orientation; with available GNSS data for this deep-focus earthquake, the only values confidently determined are parameters characterizing an equivalent point source. In other words, due to the focal depth and station network configuration, all the GNSS stations are in the far-field.

The fault center or the source point is (1) assumed as GCMT centroid (Shestakov *et al.*, 2014), (2) found for the best solution as about 60 km southeast from the GCMT centroid (Steblov *et al.*, 2014), or (3) assumed as NEIC PDE coordinates of the epicenter for the dynamic case and GCMT centroid for the static case (Abubakirov *et al.*, 2015); while the  $M_0$  values are consistent: (1)  $M_0 = 4.69 \cdot 10^{21} N \cdot m$ , (2)  $M_0 = 4.25 \cdot 10^{21} N \cdot m$ , and (3)  $M_0 = (4.08 - 4.32 \pm 0.31) \cdot 10^{21} N \cdot m$ , respectively.

### 1.3.3 Main features of the aftershock sequence

The aftershock sequence of the May 24, 2013 earthquake,  $M_W = 8.3$ , consists of 94 earthquakes with magnitudes in the range of  $ML = 3.8-6.9$ . By its cumulative frequency-magnitude plot (Figure 1.16)

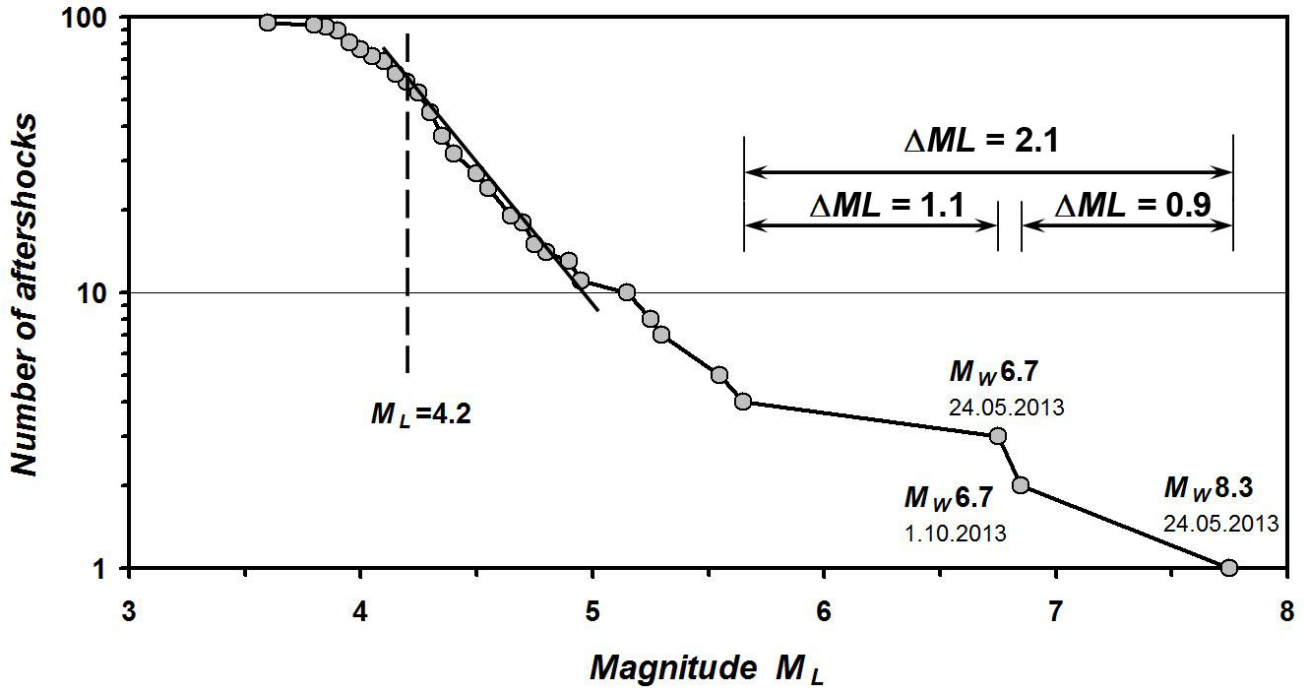


**Figure 1.16:** Cumulative frequency-magnitude plot for the aftershocks sequence of the May 24, 2013 earthquake with  $M_W = 8.3$

the catalogue completeness threshold can be determined as  $ML = 4.2$ , which corresponds to the left edge of the linear part of the curve. For further analysis 62 earthquakes that occurred prior to April 2014 were selected from the preliminary catalogue based on this threshold.

Figure 1.10 shows an ellipse containing 90% of the aftershocks for the first 14 hours after the major earthquake, allowing to estimate the rupture area of the May 24, 2013 earthquake,  $M_W = 8.3$  as 400 km (length)  $\times$  180 km (width).

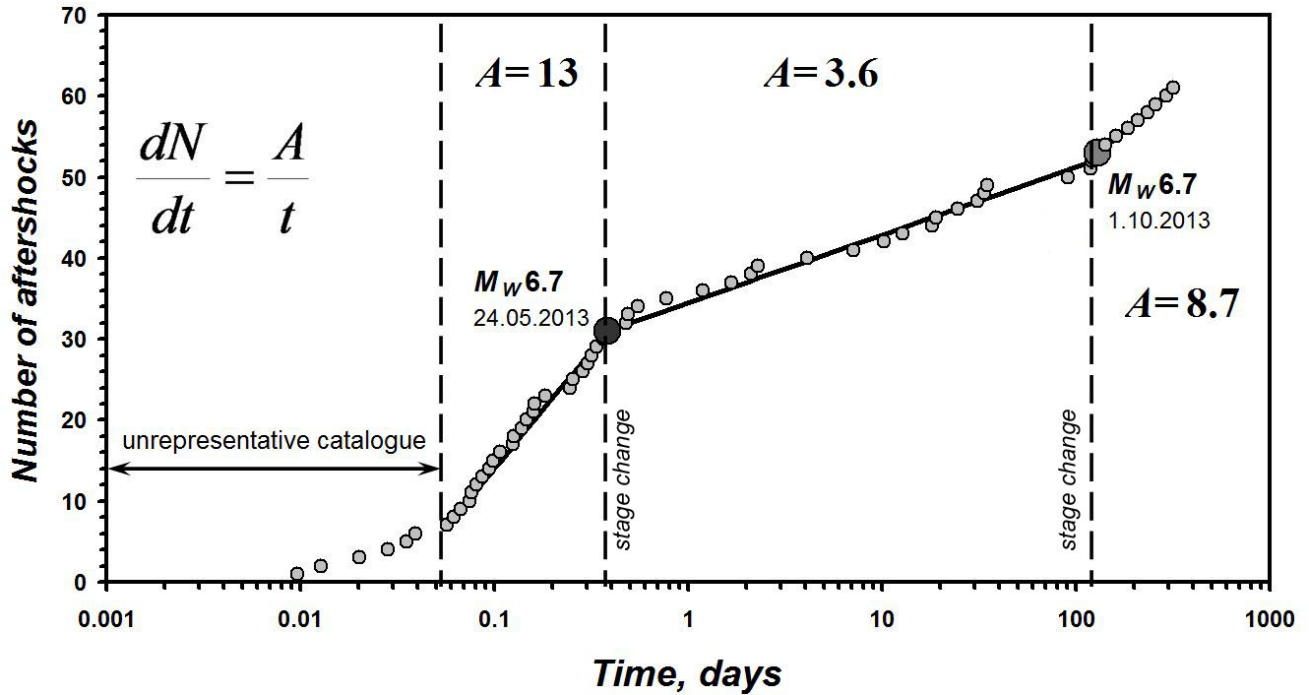
According to the frequency-magnitude plot (Figure 1.16) the energy interval between the main event and the strongest aftershock  $\Delta ML = 0.9$  is comparable to the interval between the two strongest aftershocks and a relatively numerous group of aftershocks with a continuous energy distribution ( $\Delta ML = 1.1$ ).

Figure 1.17 shows the cumulative number of aftershocks over time in logarithmic time scale. The aftershock sequence can be divided into several stages based on the change of the slope of the plot.

First of all, it is necessary to exclude the initial stage with a duration of an hour and consisting of 6 aftershocks with magnitudes between  $ML = 4.4$ - $5.3$  from consideration because we believe that powerful coda-waves of the main shock could have masked several events.

The remaining sequence of earthquakes can be divided into three stages, each of which is approximated by a straight line on the plot of Figure 1.17 that has a semi-log scale. This approximation corresponds to a hyperbolic decay of  $dN/dt$  where the slope of the line is represented by a proportionality coefficient  $A$ . Note that the last segment of the hyperbolic-law approximation is less reliable because of the small amount of data.

A peculiar feature is the coincidence of the two stage changes and the two most powerful aftershocks with magnitude  $M_W = 6.7$  each: on May 24, 2013 (9 hours after the main shock) and on October 01,



**Figure 1.17:** The typical stages of the aftershock process of the May 24, 2013 earthquake,  $M_W = 8.3$ . The starting point corresponds to the main event origin. Time bounds of the stages with linear trends are indicated.

2013 (after >4 months). None of these earthquakes triggered its own aftershock sequence.

It should also be noted that the May 24, 2013 earthquake with  $M_W = 6.7$  at the end of the most intense part of the aftershock sequence occurred outside the ellipse containing 90% of aftershocks of the  $M_W = 8.3$  earthquake, and it can be alternatively qualified as a separate event, not as an aftershock in a narrow sense (№12 in Figure 1.10).

### 1.3.4 Macroseismic data

Macroseismic information was collected for 190 settlements. From various sources, 546 responses were processed, of which 90 messages of 29 sites were received through the Internet-based questionnaire (<http://www.emsd.ru/lsopool/poll.php>).

The Sea of Okhotsk earthquake on May 24, 2013 had a great area of macroseismic impact, while it nowhere had any catastrophic manifestations. This event was felt with intensities up to VI degrees on the MSK-64 scale in the settlements located from the epicenter at distances from 139 to 9470 km. In the northern hemisphere of the Earth on a significant part of Eurasia and North America its effect was reported in Russia, Kazakhstan, Japan, China, India, the United Arab Emirates, Poland, Canada, the USA, Mexico, Italy, Estonia and Kyrgyzstan; in the southern hemisphere - in Indonesia on the Java island.

In the Kamchatka area macroseismic data from 64 settlements, were collected. In 50 of them the earthquake was reported to be felt with intensities of II to VI degrees (Figure 1.18). The nearest site to the epicenter, Krutogorovo village, and other towns of the western coast of the Kamchatka Peninsula reported intensities of no more than IV degrees, with the exception of the Oktiabrsky village ( $I = V$



degrees). The strongest ground shaking was reported in areas of the eastern coast: I = VI degrees on the Semyachik meteorological station and in the Valley of Geysers, I = V-VI degrees at the Krugly lighthouse. Thus, the highest intensities were reported close to the deep sea trench. This feature is typical for deep island arcs earthquakes, and was first seen in the early 20th century for events in the Benioff zone in Japan (Utsu, 1966). It was concluded that this phenomenon was caused by large inhomogeneities within island arcs.

To collect macroseismic information for the Sea of Okhotsk earthquake outside of Kamchatka official requests were sent to the Russian Ministry of Emergency Situations, all the Branches of the Geophysical Service RAS and Siberian Branch of the Geophysical Survey RAS, The Schmidt Institute of Physics of the Earth RAS, Mining Institute of the Ural Branch of RAS and other scientific institutions in different regions of Russia. Letters were sent to fellow seismologists from Azerbaijan, Kyrgyzstan, Uzbekistan, Belarus, Moldova, as well as in Kazakhstan National Data Center with a kind request to provide all the available information about the manifestations of this earthquake. There were 17 responses received out of 29 requests sent. The most detailed information was sent by A. D. Zavyalov (IPE RAS), E. P. Semenova (Sakhalin Branch of GS RAS), N. A. Gileva (Baikal Branch of GS RAS), L.I. Karpenko (Magadan Branch of GS RAS), and R.A. Diagilev (Mining Institute of the Ural Branch of RAS, Perm). In addition, information was collected from a variety of news and other Internet resources. We express our sincere gratitude to all those who assisted in the collection of macroseismic data.

As a result, in addition to the Kamchatka region, macroseismic information was obtained from 82 settlements in the territory of Russia, of which 75 reported intensities from II to IV-V degrees. The earthquake was felt by the residents of the Far East (except Primorsky region, Figure 1.19), Siberian, Volga, Central, Southern, North Caucasus and the North-West Federal District (FD) of the Russian Federation.

In Russia, outside Kamchatka, the strongest ground shaking with I = IV-V degrees were reported at two sites: Severo-Kurilsk and Gornoe in the Sakhalin region. Shaking of the intensity of IV was felt in the city of Magadan and Klepka in the Magadan region, Ulegorsk, Aniva, Tymovskoe and Troitskoye in the Sakhalin region. In Moscow and Khabarovsk the earthquake intensity manifestations varied from II to IV, obviously, depending on the soil type and construction quality. In other Russian towns the earthquake was felt with almost equal intensity of about II to III. From Kazakhstan National Data Center macroseismic information was obtained for 7 settlements located on the territory of Kazakhstan, which allowed to specify the data featured at the US Geological Survey (USGS) (<http://earthquake.usgs.gov/earthquakes/dyfi/>).

According to information received from the Seismological Service of Moldova, Belarus and Azerbaijan, the earthquake in these countries was not felt. On the website of the European Mediterranean Seismological Centre (EMSC) (<http://www.emsc-csem.org/Earthquake/Testimonies/comments.php?id=318696>) testimonies of the Sea of Okhotsk earthquake from Estonia, Italy, Kyrgyzstan are available. However, intensities are not available.

Figure 1.19 also provides information about macroseismic manifestations in different areas of the world, compiled by the US Geological Survey (USGS) using their DYFI system (Did You Feel It?) (Wald *et al.*, 2011). Texts of received questionnaires were kindly provided to us by the USGS employee, D.J. Wald. The analysis of the text messages received allowed assessing ground shaking intensities at these

---

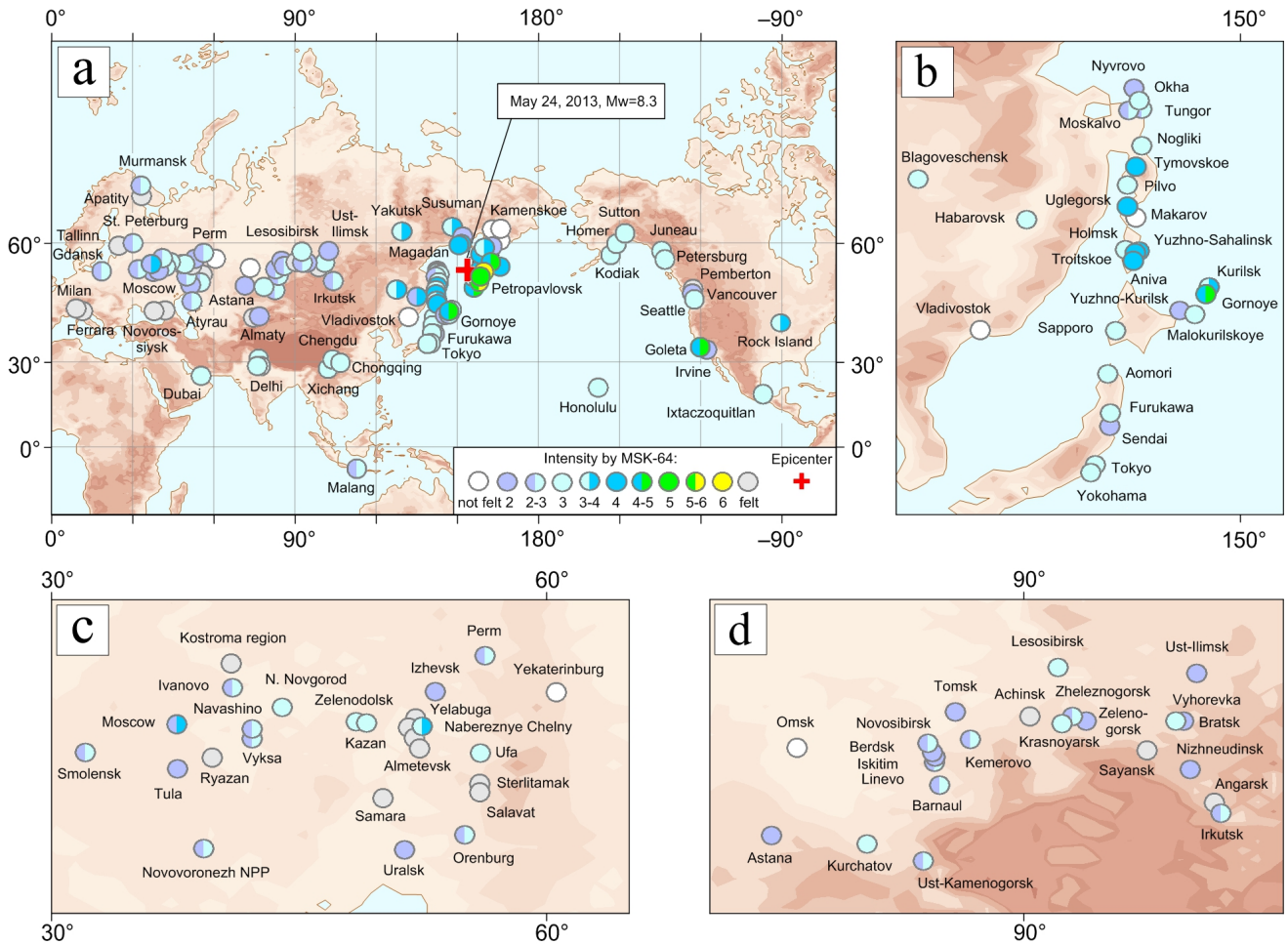


**Figure 1.19:** a) Macroseismic map of the Sea of Okhotsk earthquake on May 24, 2013 (MSK-64 intensity scale). More details: b) Japan - Sakhalin - Primorye, epicentral distances,  $\Delta = 10-20^\circ$ ; (C) Central Russia - Ural,  $\Delta = 50-60^\circ$ ; (G) Siberia - North Kazakhstan,  $\Delta = 30-40^\circ$

sites using the MSK-64 scale (Medvedev *et al.*, 1965). In most reports the intensities do not exceed III. Only in the United States there were 2 sites with more notable shaking: the greatest intensity with I = IV-V degrees in Goleta and with I = III-IV degrees in the city of Rock Island, IL.

Thus, macroseismic effects of the 2013 Sea of Okhotsk earthquake were manifested globally. It was felt in almost all major cities of Russia and caused a considerable interest of seismologists. Macroseismic effects of the Sea of Okhotsk earthquake are studied in a number of papers, for example, Zhigalin *et al.* (2013), Tatevosian *et al.* (2014) and others. The most complete descriptions of the macroseismic impact worldwide are shown in Chebrov (2014) and Chebrova *et al.* (2015).

### 1.3.5 Conclusion

On May 24, 2013 under the Sea of Okhotsk in the area of responsibility of the Kamchatka regional seismological network, at a depth of 630 km the strongest earthquake recorded in the years of detailed observations (from 1961 to the present time) occurred with a magnitude of  $M_W = 8.3$ .

The main features of the deep-focus May 24, 2013 earthquake are:

- tectonic setting: the hypocentre is located at the north-eastern end of the Kuril-South-Kamchatka segment of the subducting Pacific plate;
- the main shock as well as the aftershocks are located near the depth limit of earthquake occurrence;
- abnormal range of macroseismic manifestations: the earthquake was felt at teleseismic distances in many settlements of Russia from Kamchatka to the territory of the East European Plain, as well as in countries of Asia (Japan, China, India and others), North America and Pacific;
- co-seismic offsets were observed at the majority of GNSS stations in Far East of Russia.

The parameters of the May 24, 2013 earthquake have been evaluated within 8 minutes from the time of registration of the earthquake within Urgent Message Service and SS TWS, which were sent to the Ministry of Emergency Situations and other relevant agencies.

In the preliminary stage macroseismic information was collected in the Kamchatka area, and the aftershock sequence was processed revealing several stages of the aftershock process.

From the aftershock distribution the rupture area of the May 24, 2013 earthquake is estimated as 400 km (length)  $\times$  180 km (width) with a depth range of 425-720 km.

Estimates of focal mechanisms produced by various methods show similar solutions.

Despite the global macroseismic effect, in nearby settlements (Kamchatka region) the earthquake was felt with intensity of up to V-VI degrees and did not cause any damages.

## 1.4 References

Abubakirov, I. R., Pavlov, V. M. and Titkov, N. N. (2015). The mechanism of the deep-focus, Sea of Okhotsk earthquake of May 24, 2013 as inferred from static displacements and broadband seismograms, *Journal of Volcanology and Seismology*, 9(4), 242-257, DOI: 10.1134/S0742046315040028.

Bormann, P. (Ed.) (2002): *New Manual of Seismological Observatory Practice (NMSOP)*, IASPEI, GFZ GeoForschungsZentrum Potsdam, Potsdam, Vol. 1-2, DOI: 10.2312/GFZ.NMSOP-2.

Chebrov, V. N., Droznin, D. V., Kugaenko, Yu. A., Levina, V. I., Senyukov, S. L., Sergeev, V. A., Shevchenko, Yu. V. and Yashchuk, V. V. (2013). The system of detailed seismological observations in Kamchatka in 2011, *Journal of Volcanology and Seismology*, 7(1), 16-36, DOI:10.1134/S0742046313010028.

Chebrov V. N. (Ed.) (2014) *Strong earthquakes of Kamchatka in 2013*. Petropavlovsk-Kamchatsky: New Book Company, 2014. 252 p. ISBN 978-5-87750-298-7. [In Russian]

Chebrova A. Yu, V. N. Chebrov, A. A. Gusev, A. V. Lander, E. M. Guseva, S. V. Mityushkina, and A. A. Raevskaya (2015) The Impacts of the  $M_W$  8.3 Sea of Okhotsk Earthquake of May 24, 2013 in Kamchatka and Worldwide, *Journal of Volcanology and Seismology*, 9(4), p. 223-241, DOI:10.1134/S074204631504003X.

- Ekström, G., Nettles, M. and Dziewonski, A. M. (2012). The global CMT project 2004-2010: centroid-moment tensors for 13,017 earthquakes, *Phys. Earth Planet. Inter.*, 200, 1-9, DOI:10.1016/j.pepi.2012.04.002.
- Fedotov, S. A. (1972). *Energy classification of the Kuril-Kamchatka earthquakes and problem of magnitude determination*, Nauka. 117 p. [in Russian]
- Fedotov, S. A. and Shumilina, L. S. (1971). Seismic hazard of Kamchatka, *Izv. Akad. Nauk SSSR Fiz. Zemli.*, 9, 3-15.
- Fukushima, Y. and Tanaka, T. (1990) A new attenuation relation for peak horizontal acceleration of strong earthquake ground motion in Japan, *Bull. Seismol. Soc. Am.*, 80(4), 757-783.
- Godzikovskaya, A. A. (2010). Macroseismic descriptions and parameters of Kamchatka earthquakes that occurred during the preinstrumental period of observation, *Journal of Volcanology and Seismology*, 4(5), 354-366, DOI:10.1134/S0742046310050052.
- Gusev, A. A., Gordeev, E. I., Guseva, E. M., Petukhin, A. G. and Chebrov, V. N. (1997). The first version of the Amax (Mw, R) relationship for Kamchatka, *Pure and applied geophysics*, 149(2), 299-312, DOI:doi:10.1007/s000240050027.
- Gusev, A. A. and Shumilina, L. S. (2004). Recurrence of Kamchatka strong earthquakes on a scale of moment magnitudes, *Izvestiya Physics of the Solid Earth*, 40(3), 206-215.
- Kondorskaya, N. V. and Shebalin, N. V. (1977). New catalog of strong earthquakes in the territory of the USSR from ancient times to 1975, Academy of Sciences, Moscow (English translation, updated through 1977, available as Report SE-31, World Data Center A for Solid Earth Geophysics, NOAA, Boulder, CO, 1982, 606 p.)
- Krashennnikov, S. P. (1949). The description of land Kamchatka, reprinted by the USSR Academy of Sciences Press, Moscow. 840 p. [in Russian]
- Levina, V. I., Mityushkina, S. V., Lander, A. V. and Chebrova, A. Yu. (2013). The seismicity of the Kamchatka region: 1962-2011, *Journal of Volcanology and Seismology*, 7(1), 37-57, DOI:10.1134/S0742046313010053.
- Medvedev, S. V., Shponhoyer, V. and Karnik, V. (1965). Scale of seismic intensity MSK-64, *Academy of Science of USSR*, 11.
- Molchan, G. M. and Dmitrieva, O. E. (1991). Identification of aftershocks: review and new approaches, *Computational Seismology*, 24, 19-50.
- Pavlov, V. M. and Abubakirov, I. R. (2012). Algorithm for calculation of seismic moment tensor of strong earthquakes using regional broadband seismograms of body waves, Bulletin of Kamchatka regional association «Educational-scientific center». *Earth sciences*, 2(20), 149-158 [in Russian].
- Pavlov, V. M. (2013). Algorithm for calculating synthetic seismograms in a layered half-space with application of matrix impedance, *Izvestiya Physics of the Solid Earth*, 49(1), 24-33, DOI:10.1134/S1069351313010102.
- Shestakov, N. V., Ohzono, M., Takahashi, H., Gerasimenko, M. D., Bykov, V. G., Gordeev, E. I.,

Chebrov, V. N., Titkov, N. N., Serovetnikov, S. S., Vasilenko, N. F., Prytkov, A. S., Sorokin, A. A., Serov, M. A., Kondratyev, M. N. and Pupatenko, V. V. (2014). Modeling of coseismic crustal movements initiated by the May 24, 2013,  $M_W = 8.3$  Okhotsk deep focus earthquake, *Doklady Earth Sciences*, 457(2), 976-981, DOI:10.1134/S1028334X1408008X.

Steblov, G. M., Ekström, G., Kogan, M. G., Freymueller, J. T., Titkov, N. N., Vasilenko, N. F., Nettles, M., Gabsatarov, Yu. V., Prytkov, A. S., Frolov, D. I. and Kondratyev, M. N. (2014). First geodetic observations of a deep earthquake: The 2013 Sea of Okhotsk Mw 8.3, 611 km-deep, event, *Geophys. Res. Lett.*, 41, 3826-3832, DOI:10.1002/2014GL060003.

Tatevossian, R. E., Kosarev, G. L., Bykov, V. V., Maciejewski, S. A., Ulomov, I. V., Aptekman, Z. Y. and Vakarchuk, R. N. (2014). Deep earthquake with  $M_W = 8.3$  was felt at a distance of 6500 km, *Izvestiya Physics of the Solid Earth*, 3, 154-162, DOI:10.1134/S1069351314030124.

Utsu, T. (1966). Regional differences in absorption of seismic waves in the upper mantle as inferred from abnormal distributions of seismic intensities, *Geophysics*, 2(4), 359-374.

Wald, D. J., Quitariano, V., Dengler, L. A. and Dewey, J. W. (1999). Utilization of the Internet for rapid community intensity maps, *Seismological Research Letters*, 70(6), 680-697, DOI:10.1785/gssrl.70.6.680.

Ye, L., Lay, T., Kanamori, H. and Koper, K. D. (2013). Energy release of the 2013  $M_W = 8.3$  Sea of Okhotsk earthquake and deep slab stress heterogeneity, *Science*, 341(6152), 1380-1384, DOI:10.1126/science.1242032.

Zhigalin, A. D., Zav'yalov, A. D., Mindel', I. G., Nikonov, A. A., Popova, O. G., Rogozhin, E. A., Ruzaiкин, A. I. and Sevost'yanov, V. V. (2014). The phenomenon of the Sea of Okhotsk Earthquake of May 24, 2013, in Moscow, *Herald of the Russian Academy of Sciences*, 84(4), 283-291, DOI:10.1134/S1019331614040